END
FILMED

DTIC

AIIM

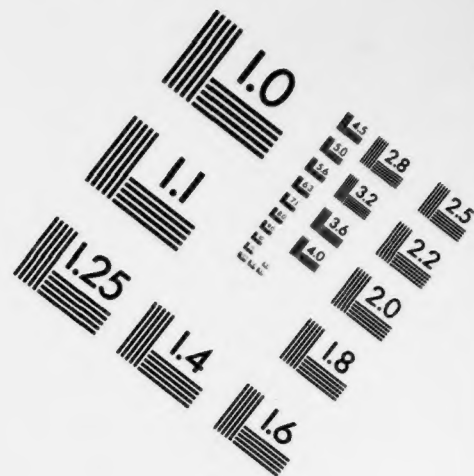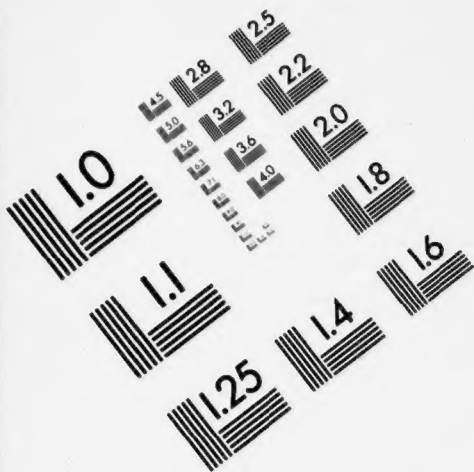**Association for Information and Image Management**

1100 Wayne Avenue, Suite 1100
Silver Spring, Maryland 20910

301/587-8202

Centimeter
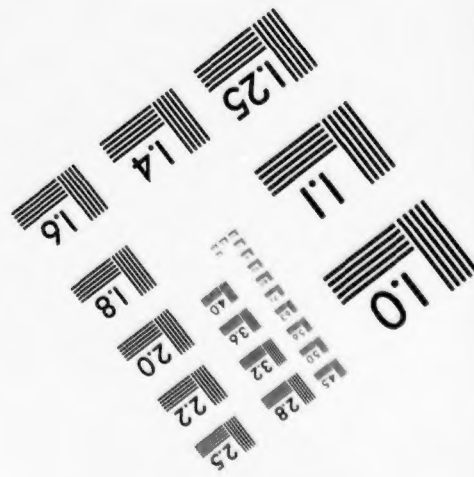
1 2 3 4 5 6 7 8 9 10 11 12 13 14 15 mm

1 2 3 4 5

Inches

1.0
1.1
1.25 1.4 1.6
1.8
2.0
2.2
2.5
2.8 3.2 3.6 4.0
4.5 5.0 5.6 6.3
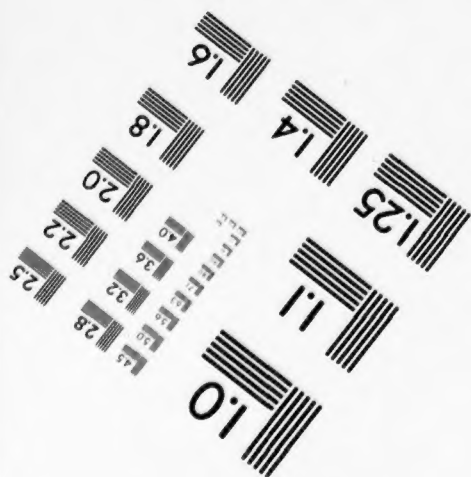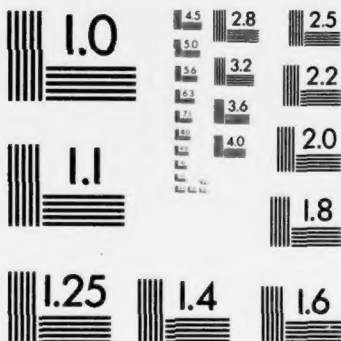
MANUFACTURED TO AIIM STANDARDS
BY APPLIED IMAGE. INC.

AARC
Atlantic Applied Research Corporation

AD-B187 443

Report Number 166

DTIC
SELECTE
AUG 0 3 1994
S
F

Pressurized Dynamic Analyzer

S. Africk
J. Hoefler
M. Caplan
E. Thalheimer

April 1, 1994

Contract No. N00014-93-C-0082

Submitted to:

Scientific Officer
Office of Naval Research| Code 1222
Ballston Tower One
800 North Quincy Street
Arlington, VA 22217-5660

Attention: Kam Ng, Code 1222

94 8 02 098   52P8 94-24416

Submitted by:

Atlantic Applied Research Corporation
4 A Street
Burlington, MA 01803

DTIC QUALITY INSPECTED 3
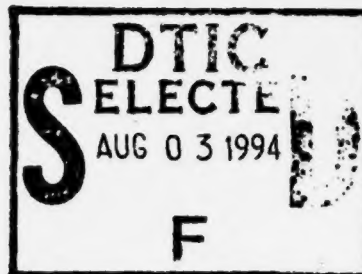
94 4 12 138

CONSULTING   DEVELOPMENT   RESEARCH

Report Number 166

Pressurized Dynamic Analyzer

S. Africk
J. Hoefler
M. Caplan
E. Thalheimer

April 1, 1994

Contract No. N00014-93-C-0082

Submitted to:

Scientific Officer
Office of Naval Research
Ballston Tower One
800 North Quincy Street
Arlington, VA 22217-5660

Attention: Kam Ng, Code 1222

Submitted by:

Atlantic Applied Research Corporation
4 A Street
Burlington, MA 01803

TABLE OF CONTENTS

LIST OF FIGURES

1. Overview

1.1 Definition

The Pressurized Dynamic Analyzer is a laboratory facility for the measurement of effective dynamic and static properties of viscoelastic material samples and their static deformation as a function of pressure and temperature. This facility will be available to the Navy and contractor community.

The device can operate with samples of solid, molded, or microvoided materials, in a variety of shapes. To date, measurements have been made on round samples cut from molded Navy tiles and commercial foamed materials; these have been relatively thin (less than one inch thick) and of 8.89 cm (3.5 in) diameter. In principle, samples as large as 25 cm (10 in) in diameter and about 30 cm (12 in) thick could also be measured using the methodology developed, although some modifications might be required with increasing size. Other types of measurements which require a controlled pressure and temperature environment are also possible. Data taken over a sufficient temperature range will be suitable for extrapolation in frequency by WLF scaling. The original Dynamic Analyzer concept is described in Ref(1).

1.2 Applications

Measurements of effective modulus can support several applications, including:

1.2.1 Coating/Baffle Design

Knowledge of effective modulus and deformation as a function of pressure allows assured predictions of coating performance. For treatments whose performance depends only on these properties, direct, definitive predictions will be possible, while for treatments with performance depending on additional factors (eg. hole resonances) the "homogeneous" parts of the layer's dynamical behavior will be measurable. This capability has not existed previously.

1.2.2 Materials Development

The analyzer can be used in support of materials development by simultaneously measuring dynamic and static properties of samples. Constitutive material properties such as Young's and shear modulus -- dynamic and static -- can be determined from the measured effective properties as long as the geometric relationships relating effective and constitutive properties are well understood. Comparisons between samples of the same geometry will not be compromised by uncertainties in these relationships.

1.2.3 Research

The analyzer can be used as a research tool to study the effects of pressure on voided coatings. For example, independent knowledge of the constitutive material properties can be combined with effective moduli and deformation with pressure to measure directly the geometrical "stiffening" of particular geometries. Investigations of these stiffening effects can be used to validate and/or correct current models and to explore novel geometries. In particular the effects of air pressure and very high levels of deformation can be explored. In addition, effects of alternative types of macrovoids and microvoids can be compared both statically and dynamically.

Another area of potential study is the effects of manufacture on constitutive properties. Relationships between these properties measured by standard practices (eg string or DMTA tests) on laboratory or production samples can be compared with values measured on completed parts to determine whether these properties are altered during manufacture.

1.2.4 Quality Control

Since the analyzer can operate with samples taken from manufactured parts, it can be used as a quality control tool for both static and dynamic properties.

1.3 Effective Modulus

The Dynamic Analyzer measures the "effective properties" of samples, which are defined as the apparent complex dilatational modulus (real part and loss factor) which defines a wave propagating with wavefronts parallel to the sample. If samples are constructed with rigid top and bottom plates, this modulus is space averaged over hole pattern.

The effective modulus alone governs the acoustic properties of most acoustic coatings. For voided materials, it is a function of the constitutive modulus of the base elastomer (complex Young's or shear and bulk modulus) and its geometry (eg. its void content or solidity). Usually the effective modulus can be expressed in terms of products of geometric terms and constitutive moduli by expressions of the type

$$\frac{1}{E_{\text{eff}}} = g_1[\phi(P)]\frac{1}{E_Y(\omega,T)} + g_2[\phi(P)]\frac{1}{B} \tag{1}$$

where g_1 and g_2 are geometric factors which depend on the geometry of the voids within a layer. In most cases, the term associated with the bulk modulus, B, is much smaller than that with the

2

Young's modulus, E_y, and the relationship between effective and Young's moduli is

$$E_{eff} = G(\phi)E_Y(\omega,T) \tag{2}$$

where $G(\phi) = 1/g_1(\phi)$ from Eq(1). This form is adequate in most cases for coatings and baffles. However, in the extreme limit of very small void content (such as may be brought on by high pressure deformation), the bulk compliance term can become important.

In these expressions, the intrinsic functional dependencies of the terms are clearly displayed: Young's modulus is a function of frequency and temperature (ω,T); the geometric factors are functions of the voids, here represented by the void content ϕ, which is itself a function of the pressure. Only B, the bulk modulus, is independent (to a good approximation) of these factors. The geometric factors, which vary with pressure deformation of a layer, refer only to the average void behavior and not to the overall layer thickness. In other words, the effective modulus is not a function of layer thickness. However, thickness is related to acoustic performance, and its variation must be included in any description of pressure effects.

A block diagram showing the relationships between coating properties and acoustical performance is shown in Fig. 1. This shows the functional dependencies in Eqs (1) and (2) and that due to thickness "feeding into" the effective modulus, which in turn determines layer acoustic properties.

The constitutive properties (ie, the Young's shear or bulk moduli) of materials are generally well measured by conventional techniques (eg. string tests, rheovibron, DMTA). Often, coating performance is predicted on the basis of these data and theoretical forms for geometrical stiffening. More recently, techniques which measure the effective moduli directly (on voided parts) have been developed, but these have not included pressure. The present facility is among the first to add this capability. It does so by measuring both:

the effective modulus

and

the layer thickness

with pressure. While knowledge of the latter is necessary to make coating performance predictions, as shown below (Sec. 3.1) it is also necessary to measure thickness in order to determine the effective modulus.

1.4 Range of Operation

The ranges of operation over which the Pressurized Dynamic Analyzer is designed to operate are:

frequency: 10 to 1000 Hz
pressure: 0 to 8.6 MPa (0 to 1250 psig)
temperature: Room Temperature to 93 °C (200 °F)

1.5 Principles of Operation

The dynamic analyzer is essentially a shake table. The sample is mounted horizontally on an approximately conical holder attached to a shaker. A metal "mass" plate is mounted above the sample. The ratio of the velocity of the shaker and that measured by an accelerometer mounted to the mass plate is the primary measurement. This transfer function (magnitude and phase) is related to the complex effective modulus by the model derived in Sec. 3.1. This model is a full wavebearing formulation which is in principle capable of handling samples of arbitrary thickness.

For thin samples, the transfer function typically has the form of a simple resonance, with a peak value at a frequency determined by the stiffness of the sample and the mass of the top plate and a magnitude governed by the inverse of the loss factor. The phase passes through 90° at a frequency close to that of the peak. Experience has shown that the best data are those near the peak, where signal to noise ratio is highest, giving each measurement with a single top plate mass a limited bandwidth. This limitation can be overcome by the use of multiple top plate masses. However, the algorithms used (Sec. 3.2) are valid away from these frequencies and depending on signal-to-noise, data analysis over a wide frequency range is possible.

Sample thickness deformation is measured by a Linear Variable Differential Transformer (LVDT). This device has a moveable probe which contacts the center of the sample. Displacement of this probe through coils within the body changes the electrical impedance and is read by a calibrated circuit. In this manner, the movement of the sample top plate is monitored as a function of pressure.

1.6 Motivation for gas pressurization

Deformation of coating samples in devices of this nature can be achieved in three general ways, pressurization by liquid or by gas, and mechanically. The selection of gas pressurization

4

was made on the basis of simplicity. In either of the two other possible approaches, it is very difficult to assure that the medium does not cause a mechanical "short circuit" by introduction of spurious paths over which mechanical energy can propagate. With gas, it alone is in contact with the sample and this possibility is eliminated. This design is clearly the best from the standpoint of dynamics.

The major problem with gas is safety, as a pressure vessel containing gas at hundreds of psi contains a great deal of energy. To minimize any danger, the vessel is constructed according to ASME standards and all penetrators are pressure rated. As long as requisite care is consistently taken during its operation, the PDA will be safe.

2. Physical System Description

2.1 Dynamic Analyzer Section

The actual analyzer, which is shown in Figure 2, is a unit which consists of a Wilcoxon Research Inc. F4 low frequency (i.e. 10 Hz to 10 kHz) electromagnetic shaker, fitted with a conical aluminum insert. The conical aluminum insert is added to allow a uniform force to be applied to a 3-1/2" diameter sample. A sample is then placed on top of the aluminum cone and then a 3-1/2" diameter aluminum plate, with known mass, is placed on top of the sample. Accelerometers are mounted vertically on both the bottom conical insert and the top mass. The accelerometer signals are then amplified and retrieved by an HP 3560 dual channel analyzer. The analyzer is also the supplier of a swept sine wave input to the F4 shaker.

Both the sample and the top mass plate were held together using vacuum pump oil. The technique used involved applying the oil to both surfaces and pressing the two surfaces together tightly. The excess oil that "squeezed out" was then wiped clean and the samples were held from the capillary forces.

2.2 Environmental Control Chamber

The dynamic analyzer described in the previous section was placed within a pressure vessel designed to work up to 1250 psig. The entire analyzer assembly was placed within the vessel and sealed. All electrical connections such as the shaker power, accelerometer signals, LVDT signals, etc. were made by passing the cables through NPT threaded sealing glands. The glands allow cables to pass from within the pressure vessel to the ambient environment through neoprene seals located within an NPT threaded fitting. In addition to varying the pressure conditions, a heater was also mounted in the pressure vessel in order to allow for simultaneous temperature control.

2.2.1 Pressure Vessel

As mentioned above, the pressure vessel was designed to a working pressure of 1250 psig. The vessel was built to ASME pressure vessel code specifications and is ASME code certified. The vessel, shown in Figure 3, was constructed from 16" schedule 80 pipe with 600-lbf flanges in either end of the vessel. The overall dimensions of the vessel are approximately 16 inches diameter and 21 inches in height. The approximate weight of the vessel, including top, bottom and bolts is about 2500 lbs. The top, which must be removed to replace masses, samples, etc., weighs about 450 lbs. and must be lifted and lowered with a portable crane (or chainfall etc.). The required bolt torque for sealing the gasket is 500 ft-lbs.

2.2.2 Penetrations

The penetrations built into the vessel include three of each 1/8", 1/4", 1/2", and 3/4" NPT threads. In addition, there are two openings which allow mounting of the heater coil. All cables (i.e. accelerometers, LVDT's, etc) are fed through NPT threaded sealing glands manufactured by Conax Buffalo. The sealing glands have a neoprene seal which seals around the various cables and are designed to maintain a pressure seal up to 10000 psig.

2.2.3 Pressure Control

In the experiments performed for this report, 2500 psig compressed nitrogen tanks were used to supply the pressure to the vessel. A 2500 psi regulator was used to set the downstream pressure which directly connected to one of the NPT threads on the vessel. A needle valve with a pressure gage was also connected to the vessel in order to relieve pressure when going down in experimental pressure. Presently the pressure control is a fully manual operation.

2.2.4 Temperature Control

The pressure vessel has a 1000 watt heater mounted within the vessel to allow the experiment to be performed at temperatures above the ambient. A resistive temperature device (RTD) is mounted to one of the NPT connections and monitors the temperature of the nitrogen within the vessel. The output of the RTD is connected to a PID control system which supplies the power to the heater coil. The temperature control system was supplied by Atlantic Thermal Systems, Inc. In addition, 1" thick fiberglass insulation is applied to the inside of the vessel to reduce both the heat losses and the need to include heating the vessel. The maximum temperature desired in this setup is 200 degrees F, although the heater is capable of achieving greater temperatures by reducing heat losses with the thermal insulation. The complete system (i.e. analyzer, signals, etc) is shown schematically in Figure 4.

3. Math Models and Software

3.1 Transfer Function

The algorithm used models a sample as a homogeneous material with effective space averaged complex dilatational modulus $E_{eff}(1-i\eta)$. To characterize a layer of arbitrary thickness h, the full wavebearing model is used. The complex wavespeed associated with normal propagation through the layer is

$$c^2 = \frac{E_{eff}(1 - i\eta)}{<\rho>} \tag{3}$$

where $<\rho>$ is the space averaged density. With layer characteristic impedance defined by:

$$Z_{ch} = <\rho>c \tag{4}$$

the pressures and velocity (p_1,v_1) on the face of the sample driven by the shaker and above the sample (p_2,v_2) are related by the usual four-pole matrix relation:

$$\begin{bmatrix} p_1 \\ v_1 \end{bmatrix} = \begin{bmatrix} \cos(kh) & -iZ_{ch}\sin(kh) \\ \dfrac{-i}{Z_{ch}}\sin(kh) & \cos(kh) \end{bmatrix} \begin{bmatrix} p_2 \\ v_2 \end{bmatrix} \tag{5}$$

The "bottom" equation represented by this matrix,

$$-\frac{i}{Z_{ch}}\sin(kh)p_2 + \cos(kh)v_2 = v_1 \tag{6}$$

can be rearranged to yield an expression for the ratios of the velocities in terms of the impedance p_2/v_2:

$$\frac{v_1}{v_2} = \cos(kh) - \frac{i}{(Z_{ch})}\sin(kh)\ (\frac{p_2}{v_2}) \tag{7}$$

For a purely massive top place, this ratio is

$$\frac{p_2}{v_2} = -i\omega m_p \tag{8}$$

Substituting this impedance into Eq.(7) yields the essential relationship underlying the operation of the dynamic analyzer:

$$\frac{v_1}{v_2} = \cos(kh) - \frac{\omega m_p}{Z_{ch}}\ \sin(kh) \tag{9}$$

The transfer function T is more commonly expressed by the ratio of the top velocity to the bottom; it is measured by the ratio of accelerometers, top to bottom:

$$T = \frac{a_2}{a_1} = \frac{v_2}{v_1} = \frac{1}{\cos(kh) - \dfrac{\omega m_p}{Z_{ch}}\ \sin(kh)} \tag{10}$$

Equation (10) takes on a more familiar form in the limit of a very thin layer in which the sample looks like a lumped spring. For $(kh)^2 << 1$, ie for

$$\cos(kh) \rightarrow 1 \qquad \sin(kh) \rightarrow kh = \omega h/c \tag{11}$$

8

this function takes a standard damped resonance form:

$$T = \frac{1}{1 - \dfrac{\omega^2}{\omega_o^2}} \quad where \quad \omega_0^2 = \frac{E_{\text{eff}}(1-i\eta)}{m_p h} \tag{12}$$

which can be rearranged to the more familiar form displaying the real and imaginary parts of the denominator:

$$T = \frac{1}{(1 - \dfrac{\omega^2}{\Omega^2}) - i\dfrac{\omega^2}{\Omega^2}\eta} \tag{13}$$

where the frequency Ω is defined by:

$$\Omega^2 = \frac{E_{\text{eff}}(1+\eta^2)}{m_p h} \tag{14}$$

The resonance is defined as the frequency for which the transfer function T is purely imaginary, ie, where the phase of the transfer function T is 90°. Inspection of Eq.(13) shows that this occurs for angular frequency:

$$\omega_{res} = \Omega = \sqrt{\frac{E_{\text{eff}}(1+\eta^2)}{m_p h}} \tag{15}$$

9

At this point, the magnitude of T is:

$$|T_{res}| = \frac{1}{\eta} \tag{16}$$

which is referred to as the "Q" of a simple resonant system. In general, this resonant frequency does not coincide with the maximum value of T (T_{max}), which occurs at the lower frequency:

$$\omega_{max} = \frac{\Omega}{\sqrt{1+\eta^2}} = \sqrt{\frac{E_{eff}}{m_p h}} \tag{17}$$

where the phase and amplitude of T_{max} are

$$phase(T_{max}) = \tan^{-1}\left(\frac{1}{\eta}\right) \quad and \quad |T_{max}| = \frac{\sqrt{1+\eta^2}}{\eta} \tag{18}$$

Note that the magnitude of T_{res} is smaller than T_{max} by a factor of $(1+\eta^2)^{1/2}$.

3.2 Analysis algorithm

The analysis algorithm seeks to compute the value of kh given a measured value of the transfer function through Eq.(10), which can be written in the following form:

$$T^{-1} = \cos(kh) - (kh)\frac{m_p}{M_R}\sin(kh) \tag{19}$$

where M_R is the mass per unit area of the layer (R for "rubber"):

$$M_R = <\rho>h \tag{20}$$

In terms of the measured transfer function at an arbitrary frequency T_m, the problem becomes that of finding the complex root (kh) of the equation:

$$0 = T_m^{-1} - [\cos(kh) - (kh)\frac{m_p}{M_R}\sin(kh)] \tag{21}$$

Once this root is found, the effective modulus is computed by:

$$E_{eff} = \frac{\omega^2 M_R h}{(kh)^2} \tag{22}$$

Note that, according to Eq.(22), while the product (kh) is determined by measurement, the thickness h must be known in order to compute the effective modulus of a sample. <u>As this thickness will vary with pressure, it is imperative that it be known for each pressure at which a measurement of E_{eff} made.</u>

3.3 Computer Data Analysis

The transfer function and phase data measured during the experiment is transferred from the signal analyzer to a computer. The binary information from the analyzer is translated into ASCII and then read into a MATLAB workspace which converts the three column ASCII file into a vectors of frequency, transfer functions, and phase. MATLAB script files were written to take these vectors and solve for the complex roots of Eq.(21) then solve for the modulus and loss factor according to Eq.(22). The script files ask the required information of the user such as the top plate mass, the sample density and the sample thickness. The MATLAB script makes use of the complex root solver, "FSOLVE", which is located in the standard MATLAB algorithm toolbox. The script files, including the function call which utilizes "FSOLVE", are reproduced in the appendix of this report.

In order to give an initial starting point, or "guess" to the FSOLVE algorithm, the data is scanned for the resonant frequency and its corresponding amplitude (i.e. have MATLAB search for the maximum level in the data which represents the resonance). The modulus is then estimated using Eq.(12) and the loss factor is estimated using Eq.(16). This initial estimate of the complex modulus is then passed to FSOLVE as its starting point.

3.4 Data Handling System

Essentially the sequence of information transfer which was used in this series of experiments was to accept data on the HP 3562 dual channel analyzer, use a program written in Quick BASIC to transfer the data from the analyzer to a 386 PC. Note that the data can be stored at this point on a floppy disk and analyzed on another computer. Once located on the PC, the data is converted to ASCII using another routine which was also written in Quick Basic and finally read into a MATLAB workspace. It is necessary to use a 386 PC or better in order to run MATLAB.

4. Initial Sample Measurements

Samples of U. S. Navy coatings R-91, a decoupler, and A-90, an anechoic, were kindly provided by Burke Rubber Company of San Jose, California. These were in the form of rejected tiles from a habitability treatment production run. Both samples are closed on either side by PVC cover tiles. Irregularities in these cover plies were the reason for rejection; this should not have had any effect on the static or dynamic tile properties which are governed by the macrovoided elastomer.

Samples of both tiles of 3.5" diameter were cut from the 1'x 2' tiles. Two sets of tests, static deformation and dynamic properties, were made for each samples up to 500 psi. Temperature was monitored but not fully controlled during these initial measurements.

4.1 Static Deformation

Static deformation of each tile sample was carried out using a single LVDT with measurement probe in the center of the sample, which was placed at the bottom of the pressure vessel. The upper part of the LVDT was mounted on a pressure-independent metal tripod arrangement.

4.1.1 Static Deformation of R-91

Figure 5 summarizes deflection measurements of the 1.27 cm (0.5 inch) thick R-91 sample. Two sweeps from 0 to 500 psig and back to 0 were made. There is some hysteresis, but very little drift in the LVDT readings was noted after about a minute. This is indicative of minimal creep. In this pressure range, the deflection appears to reach an asymptote of about 0.18". Set is less than 0.01". A second run up to 500 psi produced essentially the same result.

The deflections of the center of a four-layer R-91 sample in hydrostatic pressure by NUSC Ref.(2) agree reasonably well with these measurements. Deflections at the edges of these tiles were smaller.

Predictions for this deflection based on the "original" solidity stiffening model from Ref.(3) for macrovoided layers are also shown on this curve assuming static moduli of 250 (the value estimated for this material on the basis of its durometer) and 500 psi. The measured deflections are smaller in both cases. The maximum deflection of 0.18 is also smaller than the maximum predicted by theory, which is on the order of 0.25 inch. This prediction is based on the complete closing of the holes, which would reduce layer thickness by a factor of two.

The deformation of the sample is less than that anticipated on the basis of the simplest models. The holes do not close as rapidly or, apparently, as completely as the model anticipates. This may be due to the presence of the PVC cover plies, which bind the rubber where it is attached and prevent the holes from closing uniformly as modeled. The effect of the hydrostatic pressure on the edge of the sample may also contribute to its apparent stiffness.

That these data tend to agree with older data from the center of larger samples would seem to suggest that the surface binding of the rigid PVC covers is a more important factor than the sample edge effects.

If the holes do not close as rapidly as the models predict, then the solidity of the layer will not increase as rapidly as predicted, and the pressure stiffening of the tile will be slower than predicted. This is in fact the case, as is shown in Section 4.1.3 below.

4.1.2 Static Deformation of A-90

Static deflection of the 0.63 inch thick A-90 sample exhibited a great deal of creep. Figure 6 shows the deformation from zero to 500 psi and back to zero with measurements made as quickly as possible after the pressure had been changed. While this curve shows substantial hysteresis, even greater creep would have been evident had the measurements been made some time after the pressure had been changed, as the sample continued to compress after the pressure had been stabilized. Consequently, data of the type shown in Figure 6 is of limited value, as it represents only a series of snapshots of the deformation during the first pressure cycle.

The deformation of the A-90 sample with time after a step up to 300 psi is shown in Figure 7. This shows that even after an hour, the sample shows only about 90% of the total deformation measured after two hours. A simple exponential fit to this curve with relaxation time of 23 minutes is also shown. The good fit shown (especially near the long time asymptotic portion) indicates that this time scale is a good descriptor of the creep of this sample.

13

4.2 Dynamic Effective Modulus

4.2.1 Dynamic Data for R-91

Transfer functions (ratios of velocity atop and below the sample), magnitude and phase, are shown for five top plate masses vs pressure in Figures 8 through 12. The masses decrease from the heaviest (No. 1) to the lightest (No. 5) as listed in Table I

Table I

Mass No.	Mass/area
1	135.55 Kg/m^2
2	68.91 Kg/m^2
3	34.06 kg/m^2
4	17.75 kg/m^2
5	8.55 kg/m^2

For this thin sample, the approximation of a simple mass-spring system is appropriate and the peak frequencies can be thought of as increasing as $((E_{eff}/h)/m)^{1/2}$, the peak at phase 90°, and the magnitude at peak $1/\eta$. For each mass, as pressure increases, the peak moves to higher pressure, indicating greater effective modulus. The phase curves also move out with pressure, as expected.

However, these data are not of uniform quality. Consider mass No. 2 (Figure 9). The transfer functions for 0, 120 and 200 psig appear to cleanly represent a mass-resonance phenomena. At frequencies well below the peak, the ratio of the accelerometers is very close to unity and the phase is 180°. With increasing frequency, a peak is reached corresponding closely to the 90° phase point. On the other hand, the transfer functions for 300 and 400 psi start out, at lowest frequencies plotted, below 0 dB and with phase below 160°. The peaks do not align quite as well with the 90° phase points. Furthermore, these curves are shifted significantly to higher frequencies relatively more rapidly than are those at lower pressure, indicating that they may differ in some way from those taken at lower pressures. These effects are stronger for the data taken with larger masses; they are almost imperceptible for the lightest mass (No. 5).

It would appear that the higher pressure curves do not represent a simple spring-mass resonance. That they are below 0 dB at the lowest frequencies suggests that there may be perhaps another resonance at lower frequencies, and these curves are being distorted (by being pushed down to lower values) by its presence. Distortion of this type could explain the apparent rapid shift to greater peak frequencies in these higher pressure curves.

14

A potential mechanism of low frequency resonance would be a rocking motion of the top mass. That this effect seems strongest for the larger masses is consistent with this hypothesis. In the cases of some experimental runs with the heavier masses, the top plate was found to have slid to one side upon completion of the measurement and the opening of the pressure vessel. While data taken during these runs are not included here, this shifting suggests motion of the top plate consistent with a rocking resonance.

Reduced data showing the effective stiffness per unit area of the sample with pressure are shown in Figure 13. At lower pressures, the expected trend of increasing stiffness with pressure is seen, although the data for the various masses do not always line up as well as they should. This is attributed to temperature variations between measurements.

At 400 and 500 psi, all the stiffness curve segments (with the exception of those for the greatest and smallest mass at 400 psi) show stiffness decreasing with frequency, which is not a plausible result. **However, these unphysical segments correspond to those transfer functions which are judged above to not represent a simple resonance.** Furthermore, the stiffness indicated (at, say the middle of the curve segments indicative of the values at the peak of the transfer functions) appears high given the underlying trend of the lower pressure curves, which is in accord with the tendency of the offending underlying transfer functions to be shifted to higher frequencies than indicated by the trend of the lower pressure curves. Finally, the tendency of these segments to show declining stiffness with frequency may also be explained in terms of the distortion of the curves postulated above. That part of the distorted curve below the apparent peak appears to be part of a resonant curve for a higher than accurate modulus. If the curve above the peak is more representative of the actual modulus (which would be the case if the effect of the distortion decreases with frequency), then the modulus result will decrease with frequency.

Given this observation the following hypothesis can be put forward: The data which appears to represent a clean resonance peak (primarily the low pressure data) is acceptable data, and the resulting stiffness measurements are valid. Those resonance peaks which do not obey this criterion are incorrect, but still provide some information about the stiffening of the sample. For example, even though all the data at 400 psi are clearly contaminated, it is likely that the actual stiffness in the range of about 2500 psi/inch.

Figure 14 shows the area-averaged effective modulus determined by multiplying the effective stiffness by the measured sample thickness (from Figure 5). Since these values are scaled by one factor for each pressure, the shapes of the curves remain the same and the conclusions about data validity are the same. Figures 15 through 19 show the same results as depicted in Figure 14 but each plot is for a specific pressure to aide in clarity.

One unanticipated result shown here is that the effective moduli at 0 and 100 psi are about the same. (The decrease in thickness at 100 psi accounts for all of the increase in stiffness.) This is inconsistent with solidity stiffening models which predict an increase in effective modulus for all pressures. This would indicate the existence of a pressure range in which hole geometry does not vary.

4.2.2 Dynamic Data for A-90

Measurements of the transfer functions of the A-90 sample from zero to 400 psi are shown in Figures 20 through 21. These data were taken shortly (within a few minutes) after the pressure had been stabilized, so that they are likely not indicative of the long term pressure-induced deformation of the sample. It should also be noted that it was difficult to obtain data on this sample as this sample as it tended to slide off center during pressurization (as observed when removing the top off the vessel).

Unfortunately, the tendency for this material to creep had not been identified at the time these measurements were made. This suggests that the appropriate procedure should be to explore completely the static properties of a sample before making dynamic measurements. Specific methods to measure dynamics in the presence of creep appear to be required.

The transfer functions at these pressures do not show the anomalies observed in the R-91 data. All start with magnitude above 0 dB and 180° phase. The progression of the peaks appears to be slight but uniform, with the possible exception of those measured at 400 psi. These seem shifted more strongly to higher frequency, with much lower amplitude.

Effective stiffness curves are shown in Figure 22; Effective modulus curves (using the thickness derived from the static deformation data) are shown in Figure 23. Curve segments consist of data taken 15 points on either side of the transfer function maximum. These results do not appear to be physically realistic, which is not unexpected considering the degree of creep in this sample during the analyzer test.

A previous preliminary test of A90 without the pressure vessel was performed earlier in the program. The data in this sequence of tests exhibited fairly decent behavior. The transfer functions and corresponding phase data is represented in Figure 20. The reduced data for zero pressure (Figure 21) shows effective modulus increasing from about 7500 to 9500 psi in the range 800 to 2500 Hz, with loss factor increasing from slightly below 0.6 to about 0.8 in this frequency range. These values are consistent with previously measured moduli for this material. Note that the loss factors are significantly larger (and hence the loss factor data are less noisy) than those measured for R-91.

The transfer function peaks and derived moduli show only very slight increases with pressure. The quantitative significance of this result is difficult to assess in light of the material creep. It is fairly certain that the dynamic data were taken too soon after the pressure was changed to represent the ultimate deformation of the specimen. This would tend to yield underestimates of the pressure induced stiffening. However, these results are somewhat consistent with those of R-91, which showed far less stiffening than anticipated. Since the published static modulus of this material is on the order of 450 psi which is about double that of R-91, that the measured stiffening is even smaller than that of R91 may indicate that in addition to creep, there is another, common phenomenon which is limiting the pressure deformation. This could be either the binding of the cover plies or the effect of the hydrostatic pressure on the sample edges.

4.3 Comment on Stiffening Law

For both samples measured, the stiffening with pressure of the dynamic modulus is significantly smaller than anticipated on the basis of standard solidity stiffening modulus. The increase in dynamic modulii are also inconsistent with measured degradation in acoustic performance with pressure. This phenomena may be due to the pressure of the rigid cover plies or to the hydrostatic nature of the pressurization. The possibilities could be investigated by use of larger samples and with edges sealed from the pressure.

REFERENCES

1.   S.A. Africk, A. Bahlavouni, F.R. Kern, P.J. Stein "Real Time Dynamic Analyzer",
      AARC Report No. 080, October 1988

2.   E. Recine, H. Jones, "Movement of Four Layers of R91 Reflector Tile (Air-Rubber
      Baffle) Under Hydrostatic Pressure", NUSC Tech Memo No. 801125, August, 1980

3.   E.M. Kerwin, E.F. Berkman, "Unified Approach to the Technology of Thin Compliant
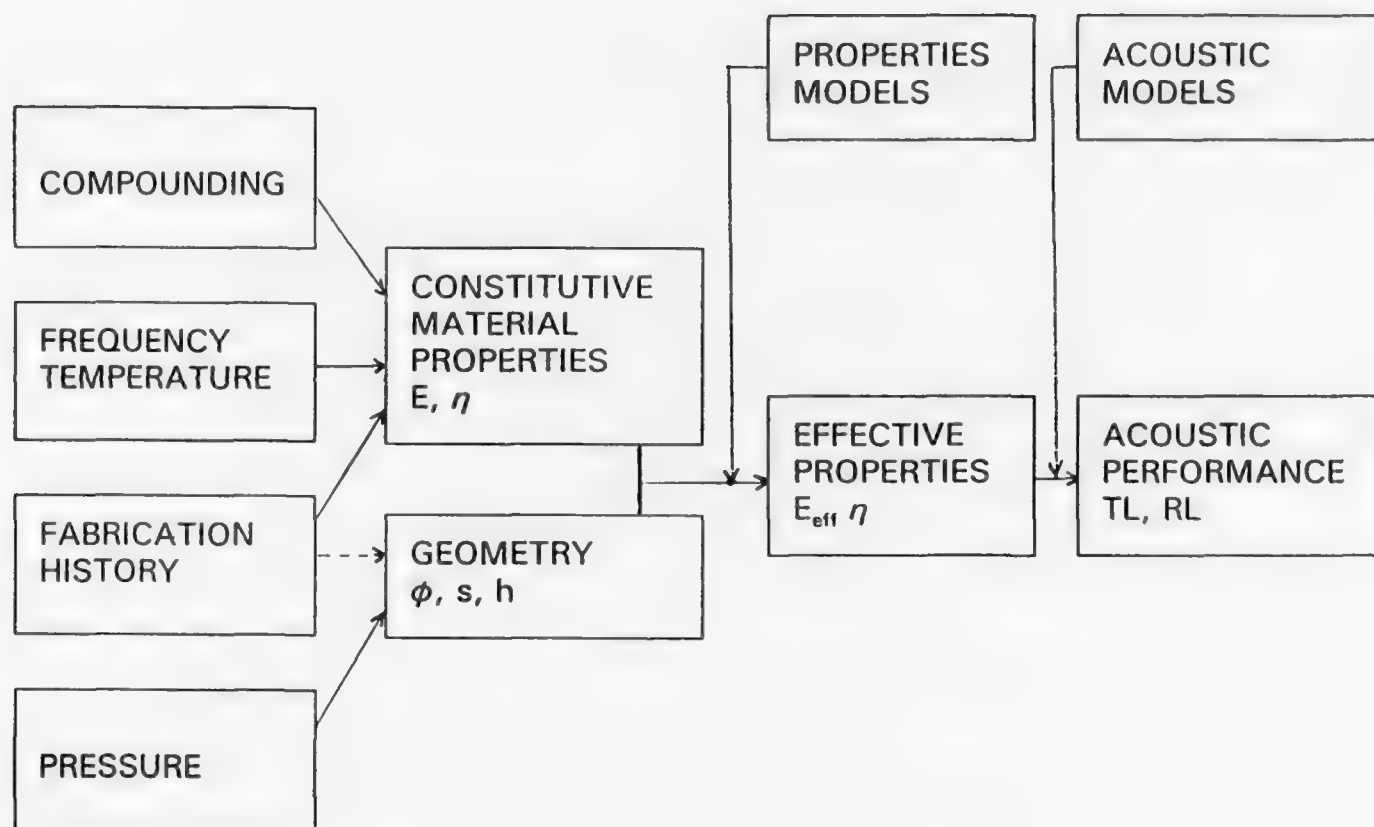   Coatings (U)", BBN Report No. 2374, June 1972 (6 Volumes) (Confidential)

Figure 1.   Relationships between Coating Properties and Acoustic Performance
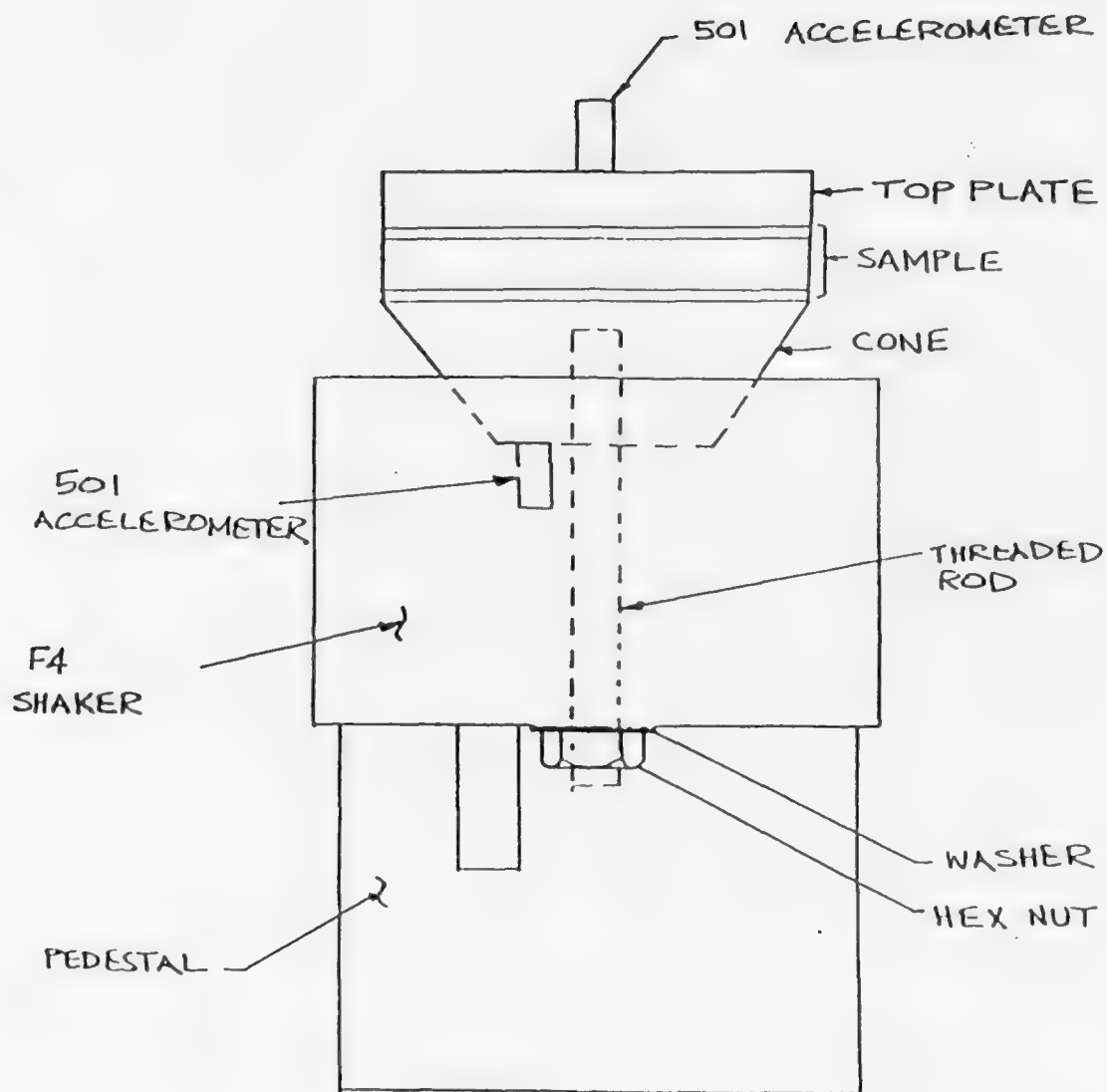
Figure 2.   Diagram of the Dynamic Analyzer
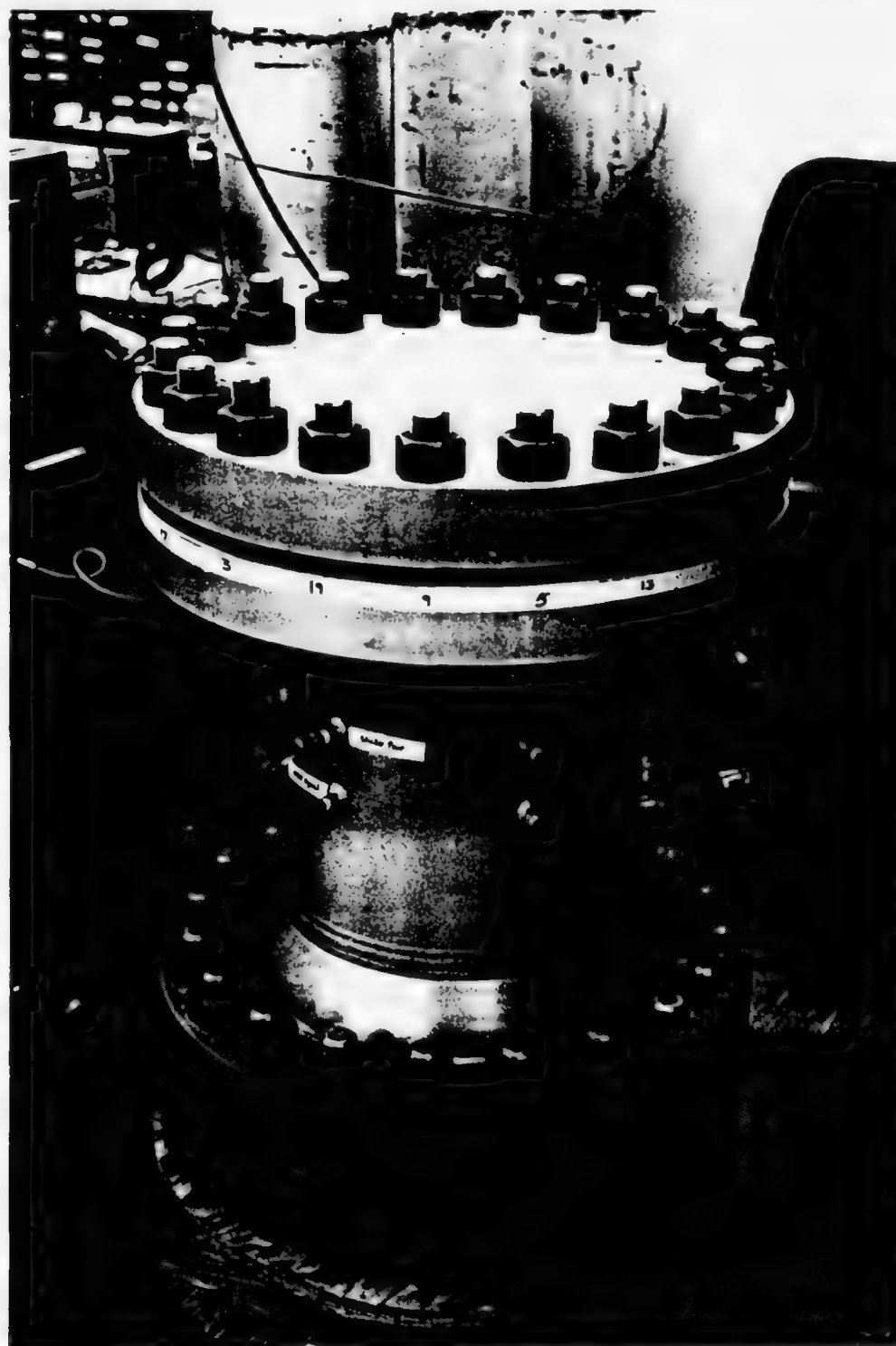
Figure 3.   Photograph of the Environmental Control Chamber
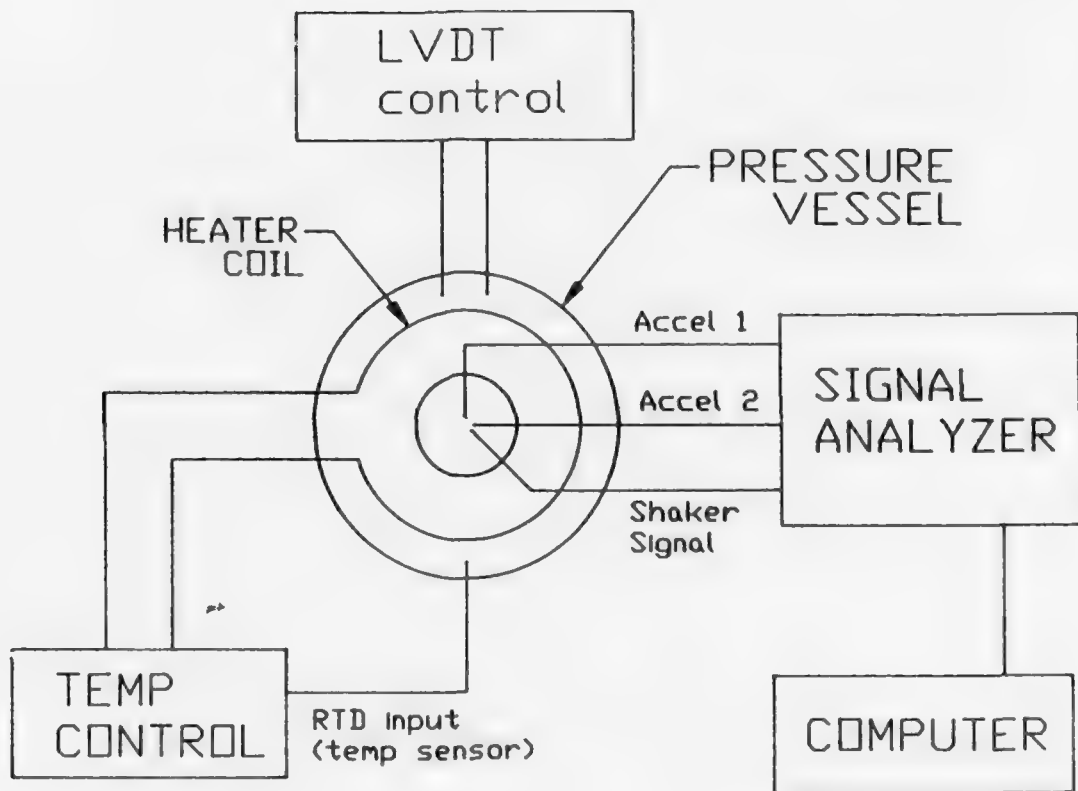
Figure 4.   Schematic of Complete System
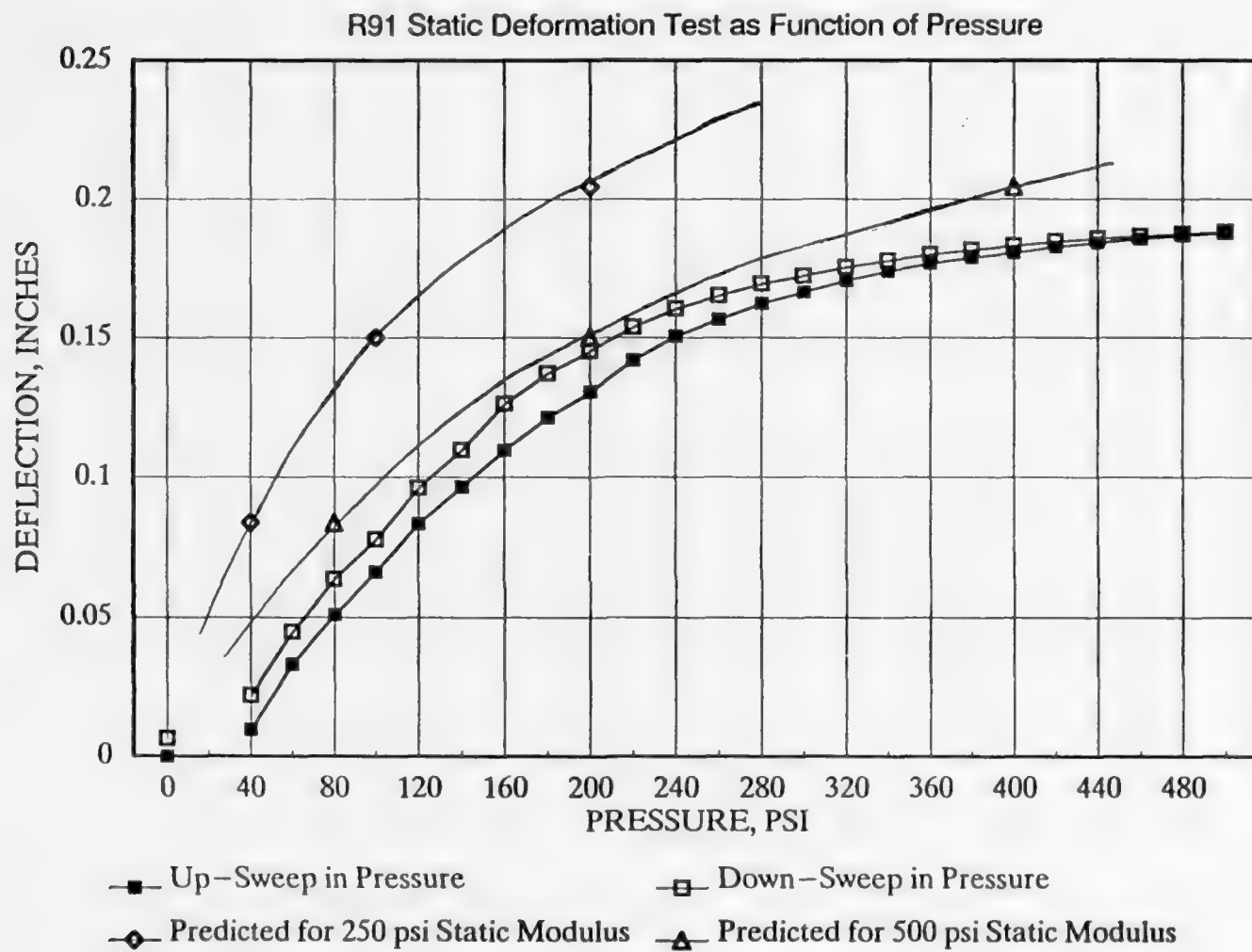
Figure 5.   Static Deformation Test of 0.5" thick R91 sample
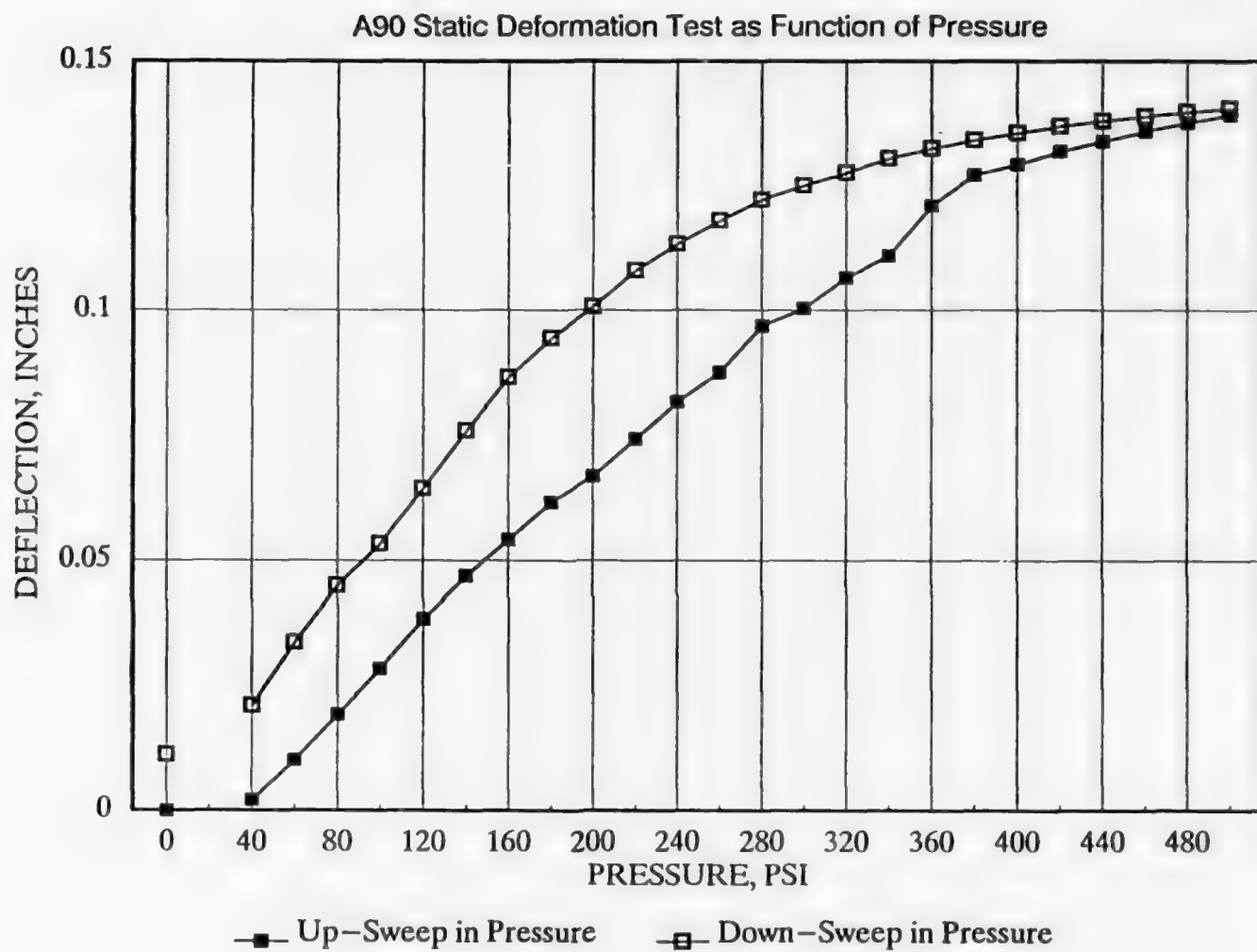
Figure 6.   Static Deformation test of 0.63" thick A90 sample
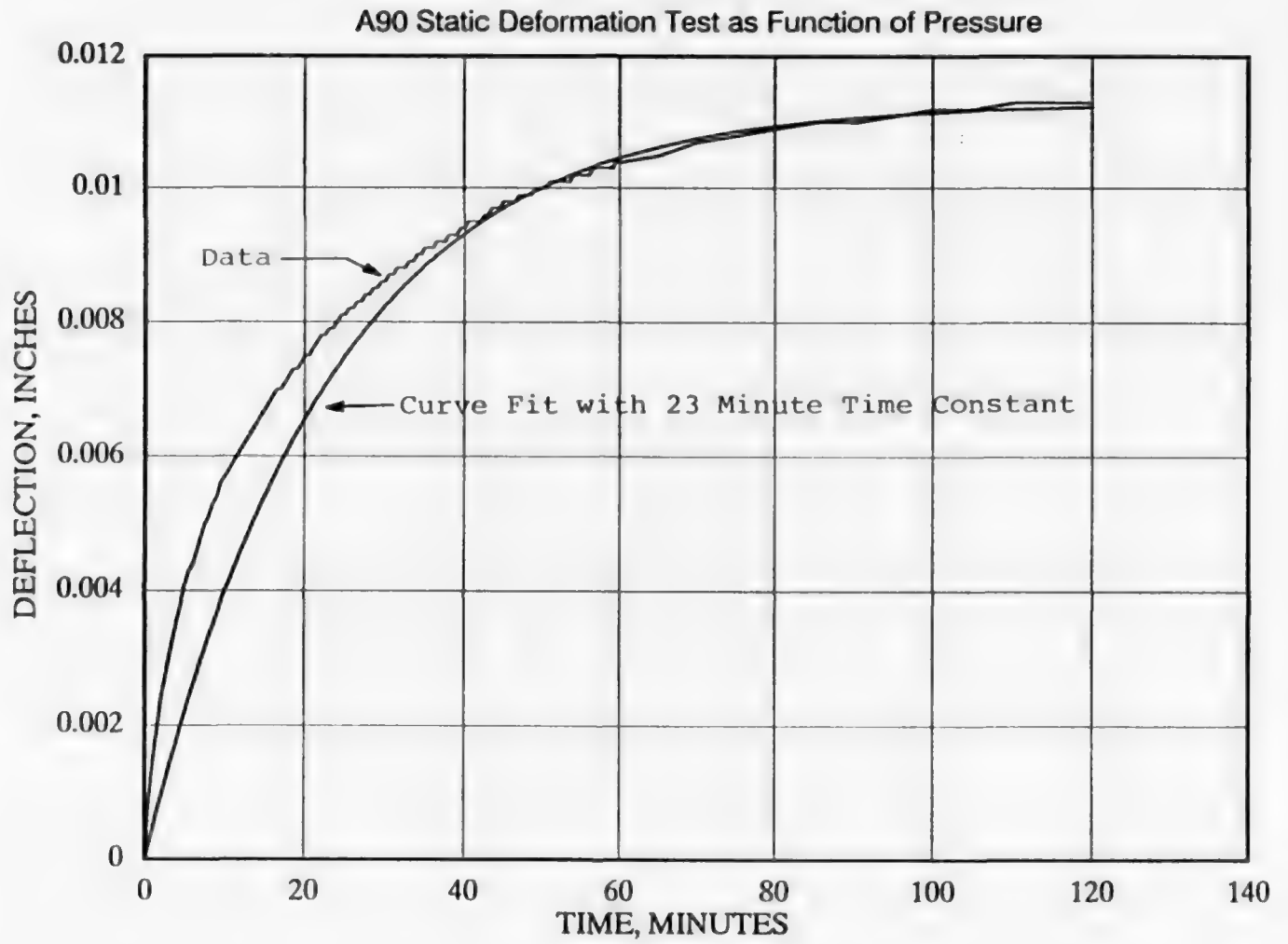
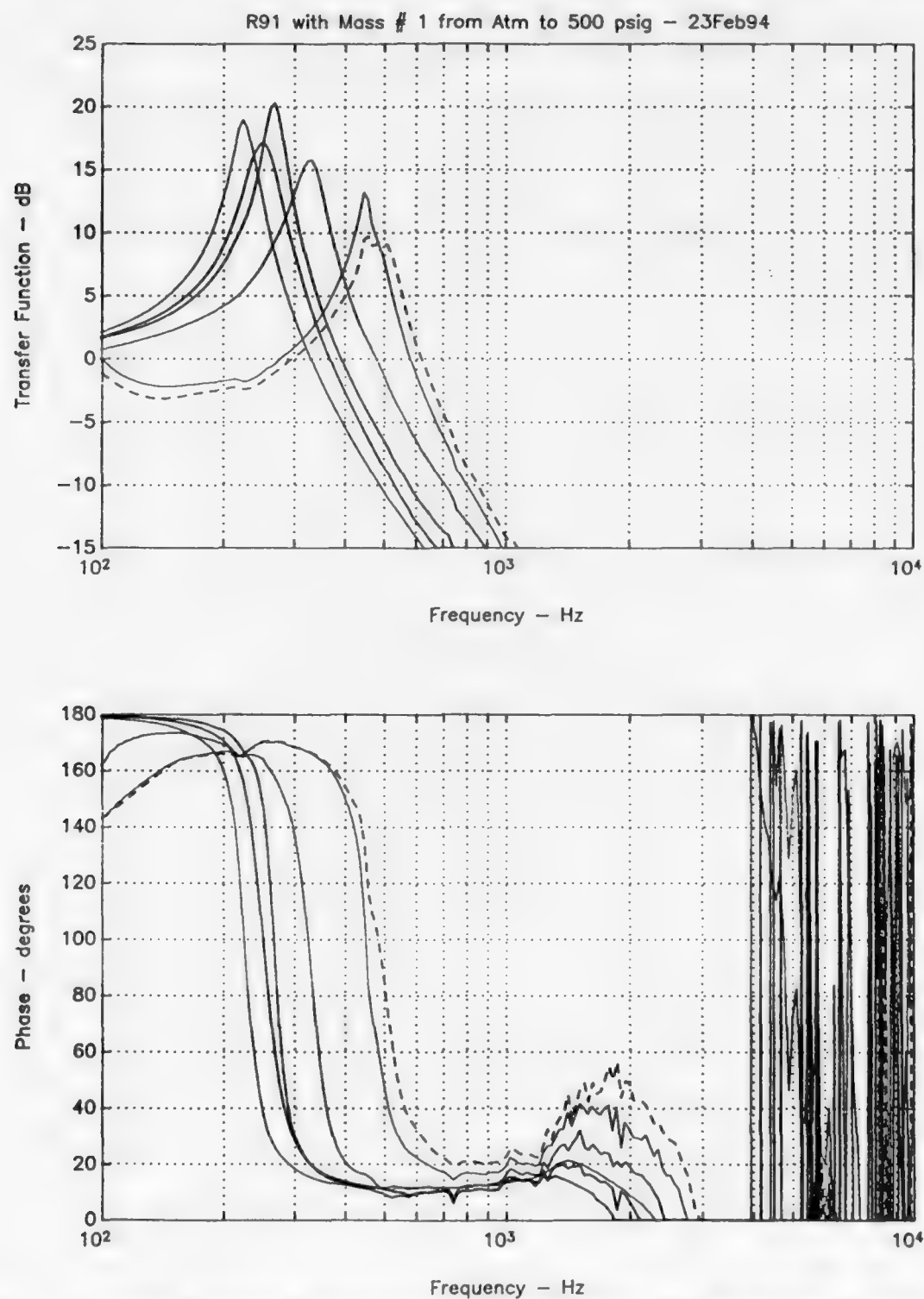Figure 7.   Static Creep Deformation Test of 0.63" A90 Sample

R91 with Mass # 1 from Atm to 500 psig – 23Feb94

Figure 8.   Transfer Function Measurement of R91 with Mass #1 from Atm to 500 psig

R91 with Mass # 2 from Atm to 400 psig – 22Feb94
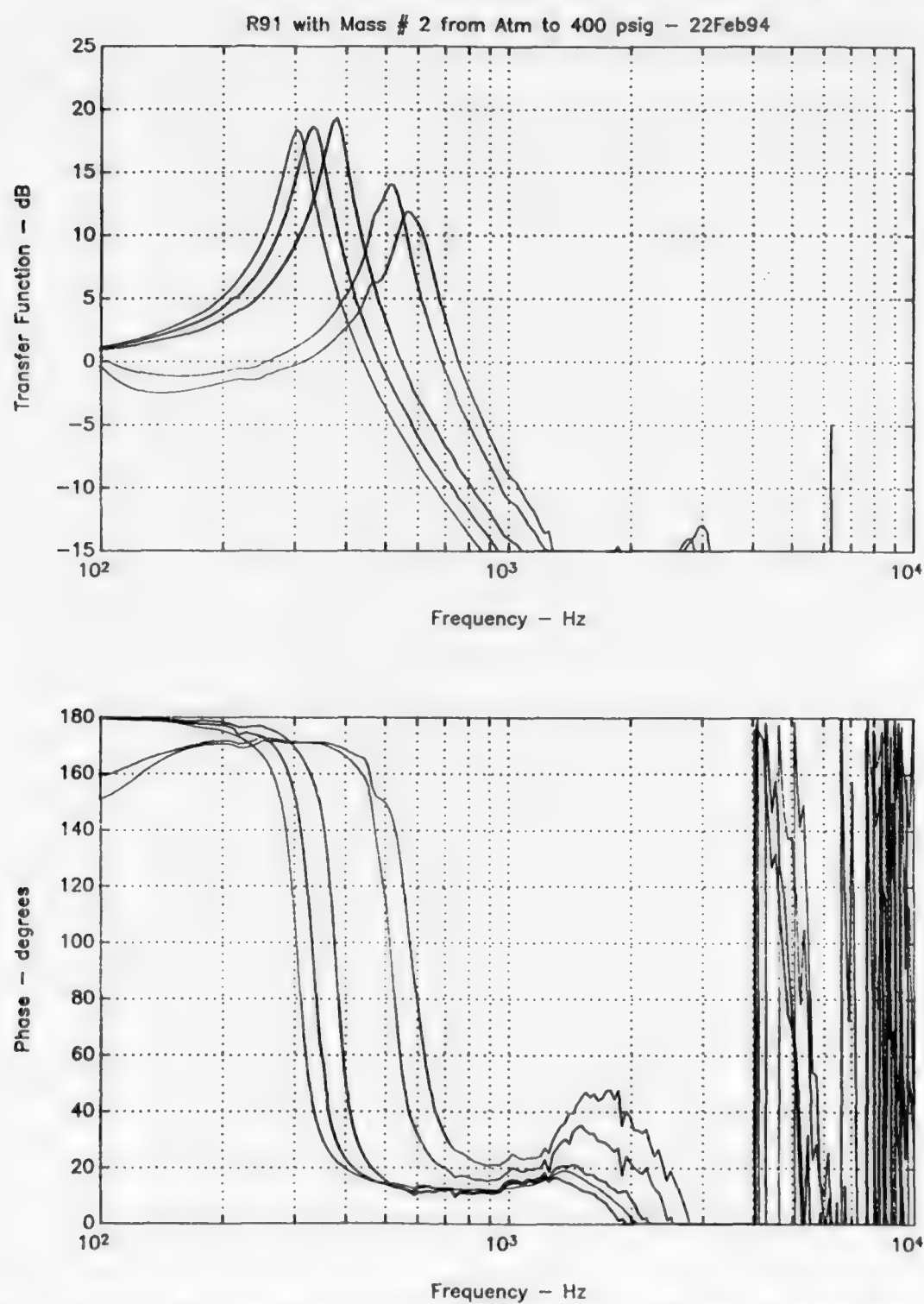
Figure 9.   Transfer Function Measurement of R91 with Mass #2 from Atm to 400 psig

R91 with Mass # 3 from Atm to 500 psig – 08Feb94
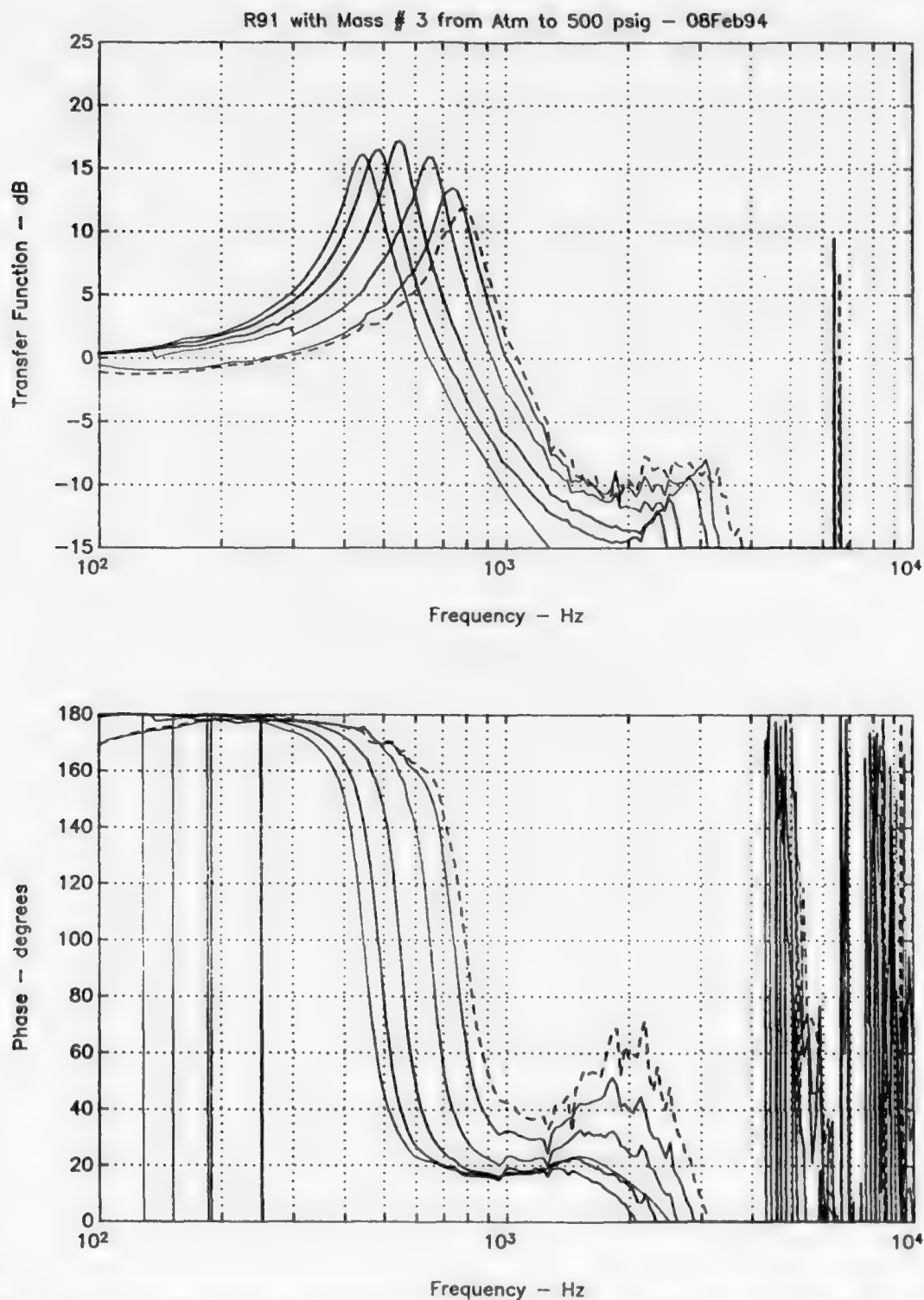
Figure 10.   Transfer Function Measurement of R91 with Mass #3 from Atm to 500 psig

R91 with Mass # 4 from Atm to 400 psig – 22Feb94
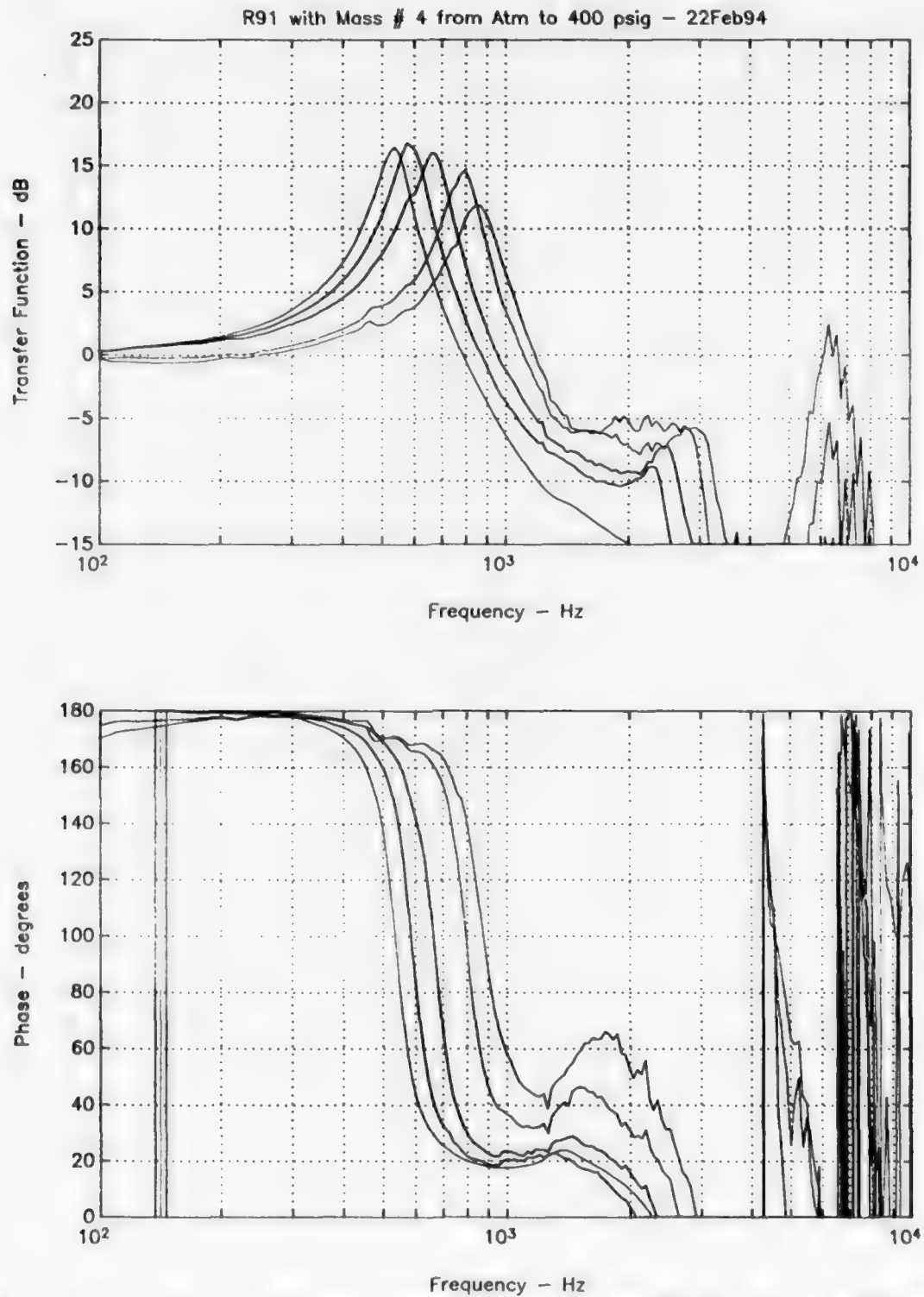
Figure 11.   Transfer Function Measurement of R91 with Mass #4 from Atm to 400 psig

R91 with Mass # 5 from Atm to 400 psig – 22Feb94
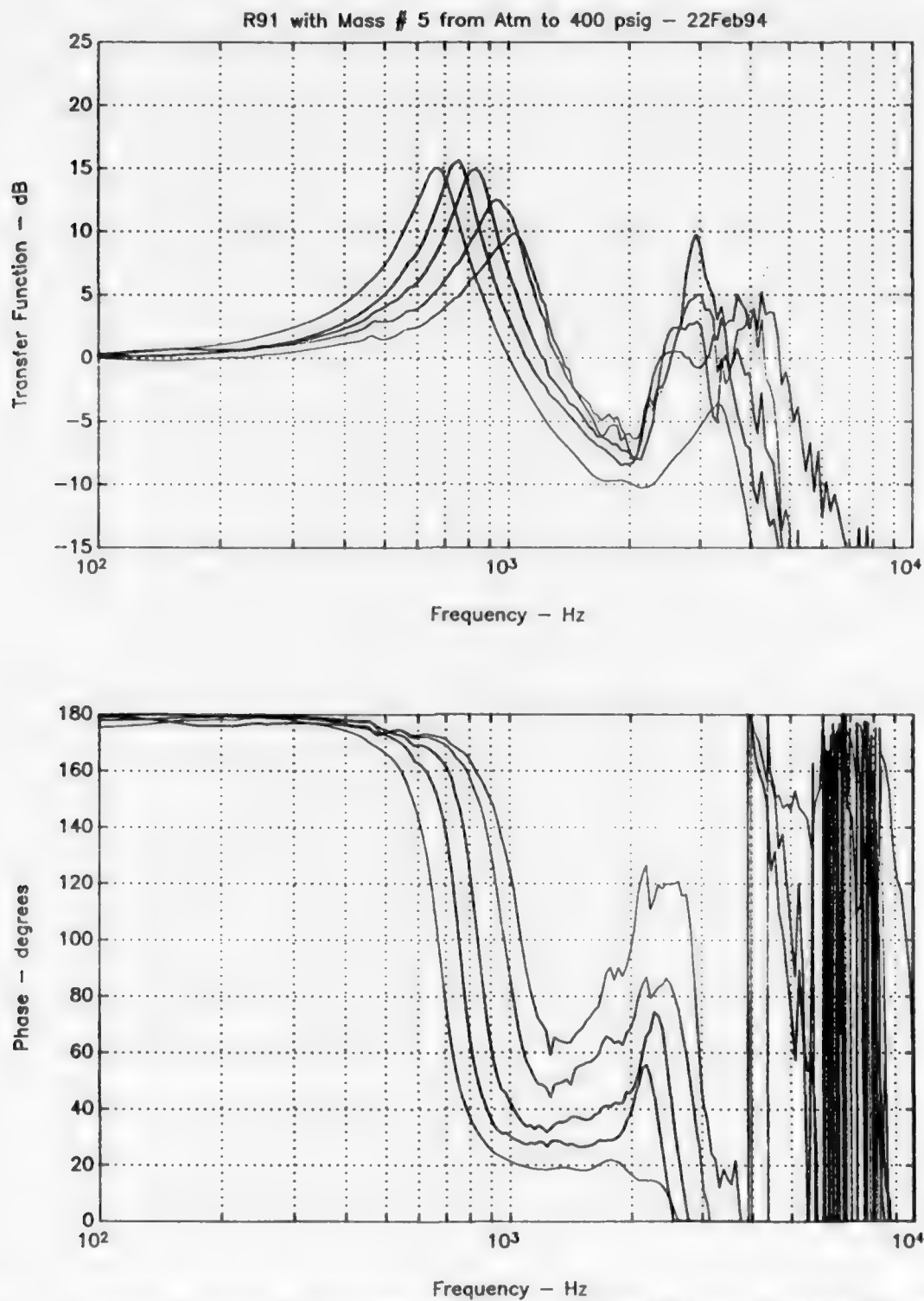
Figure 12.   Transfer Function Measurement of R91 with Mass #5 from Atm to 400 psig
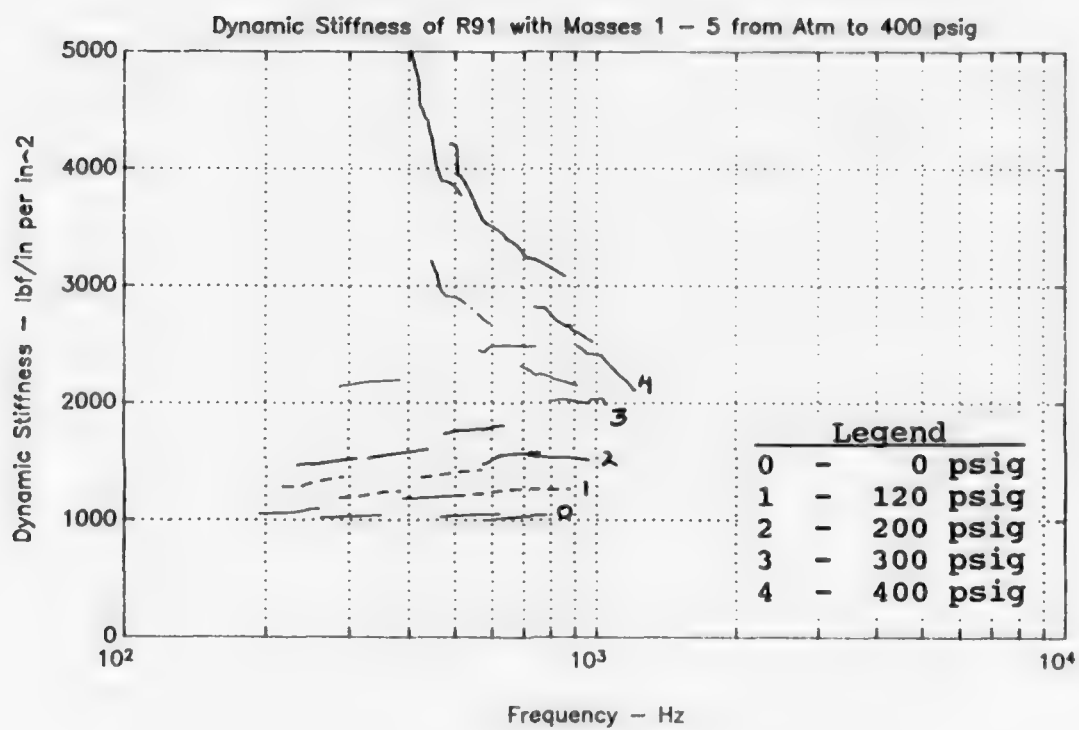
30

Figure 13.   Dynamic Stiffness of R91 with Masses 1-5 from Atm to 400 psig
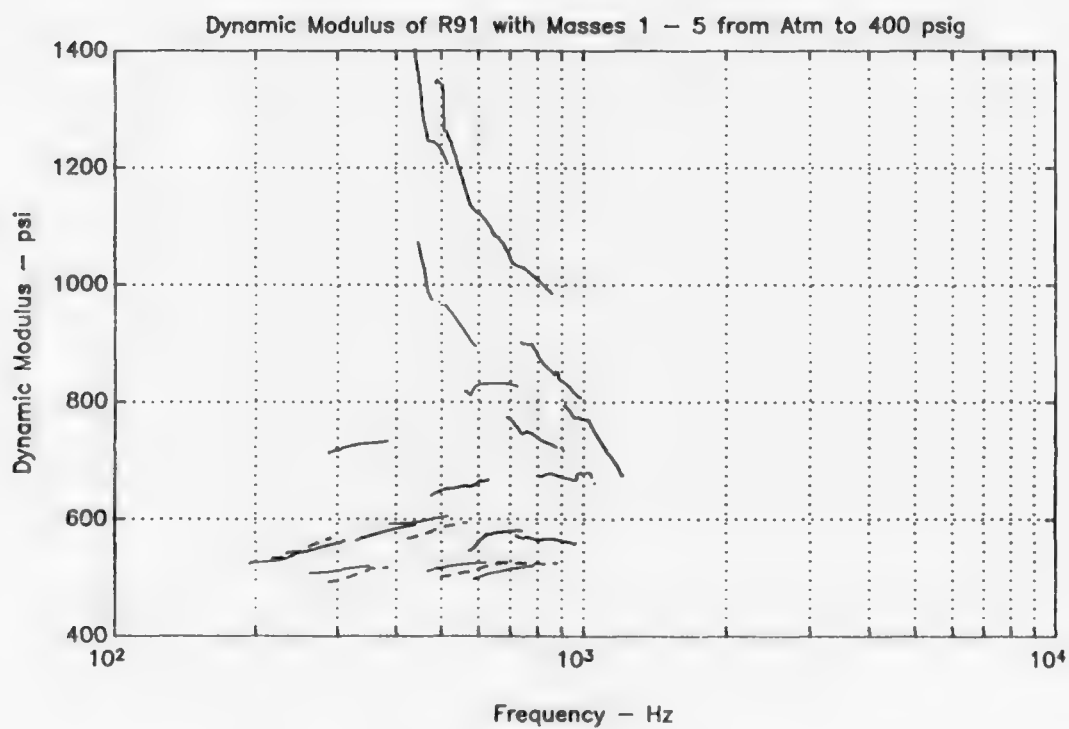
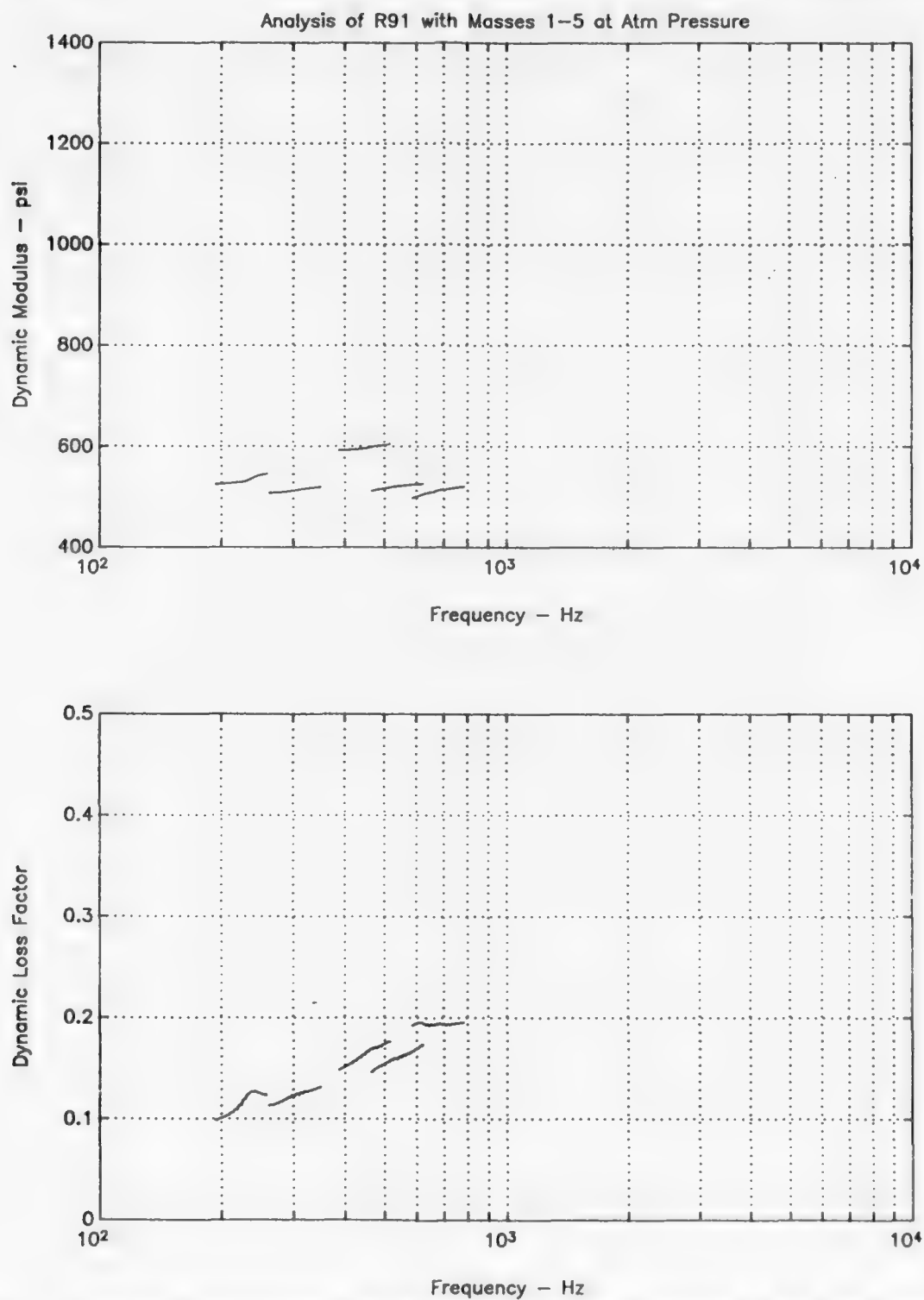Figure 14.   Dynamic Modulus of R91 with Mass 1-5 from Atm to 400 psig

Figure 15.   Dynamic Modulus and Loss Factor for R91 with Masses 1-5 at Atm Pressure

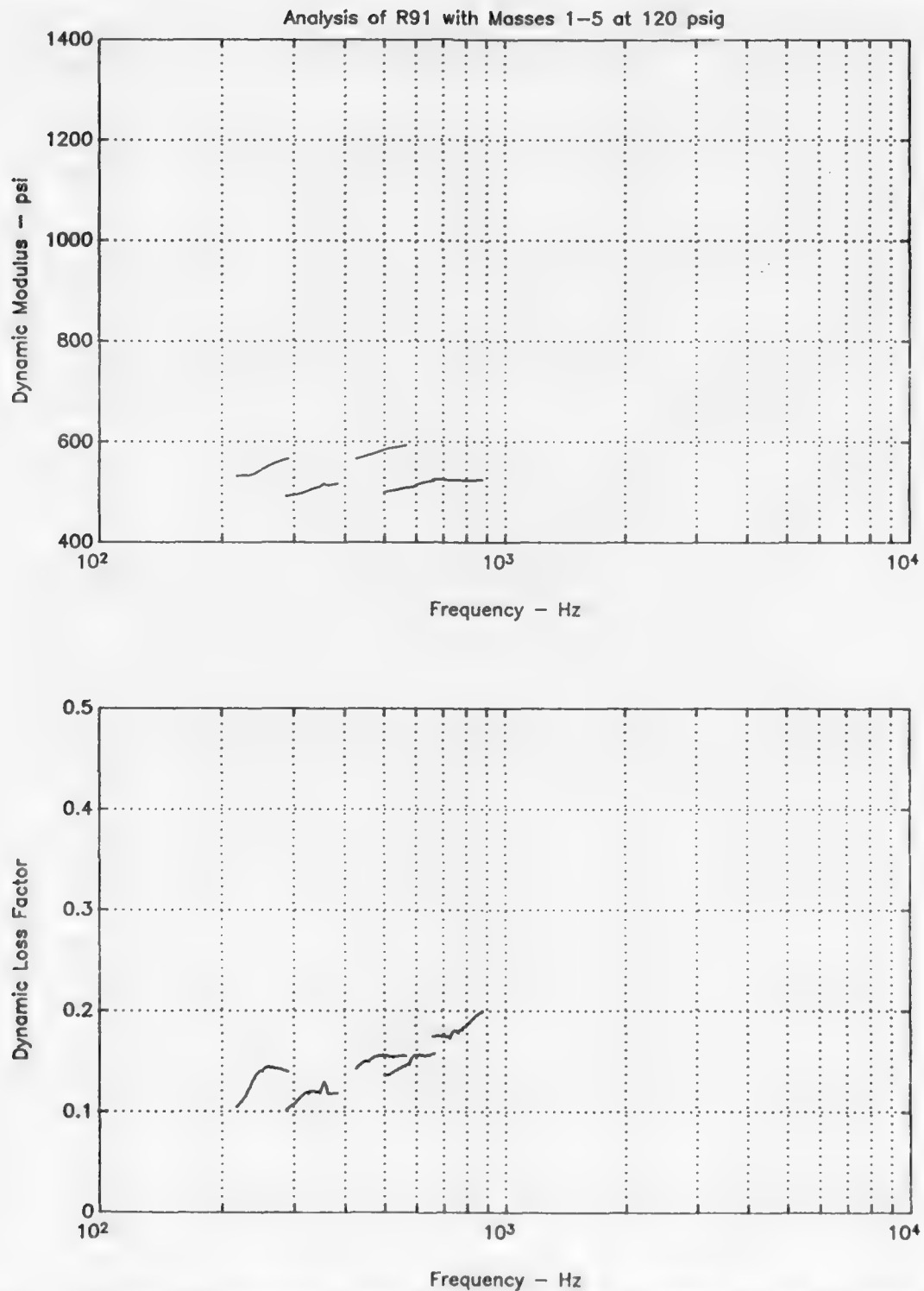Analysis of R91 with Masses 1–5 at 120 psig

Figure 16.   Dynamic Modulus and Loss Factor for R91 with Masses 1-5 at 120 psig

Figure 17.   Dynamic Modulus and Loss Factor for R91 with Masses 1-5 at 200 psig

Analysis of R91 with Masses 1–5 at 300 psig
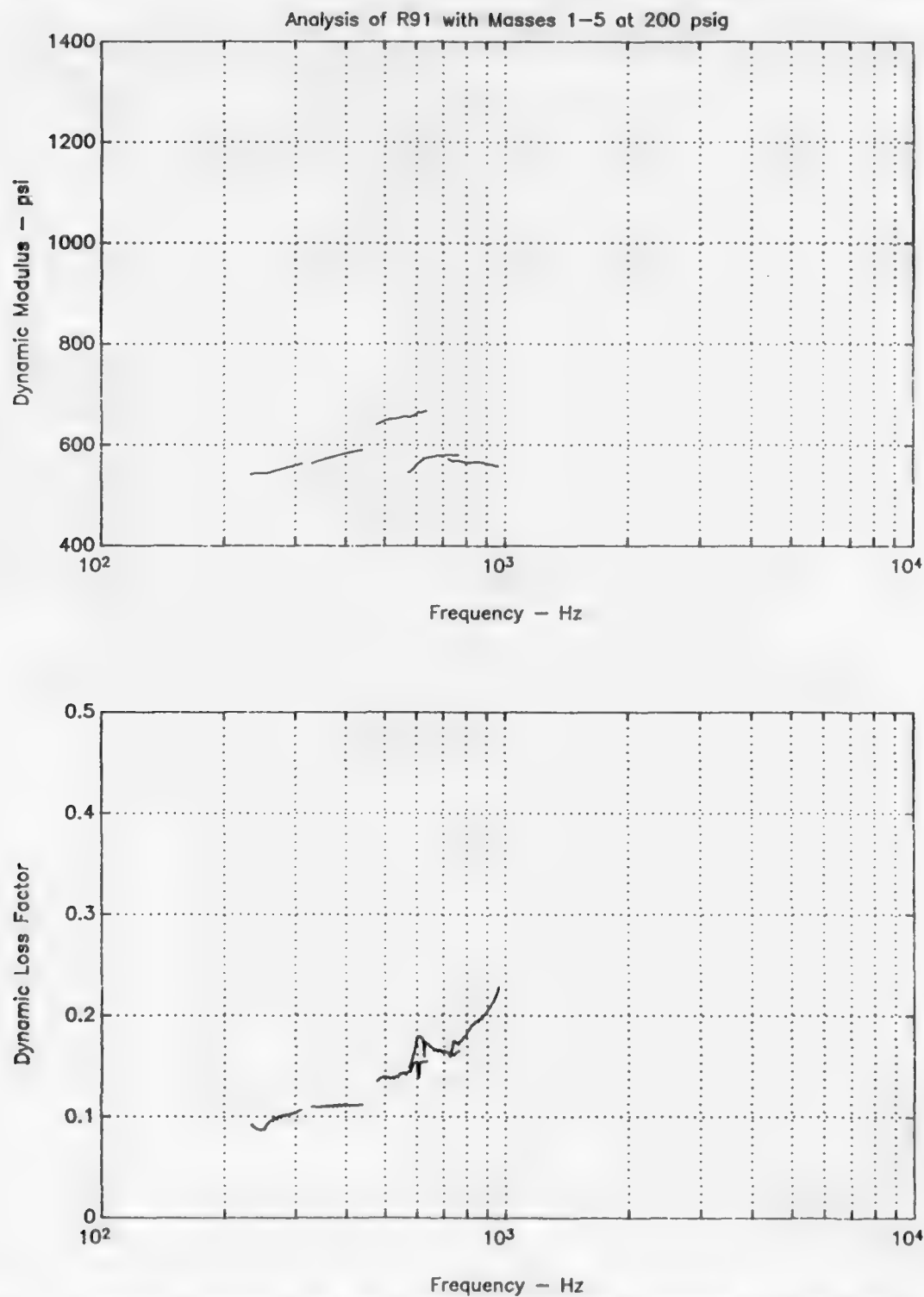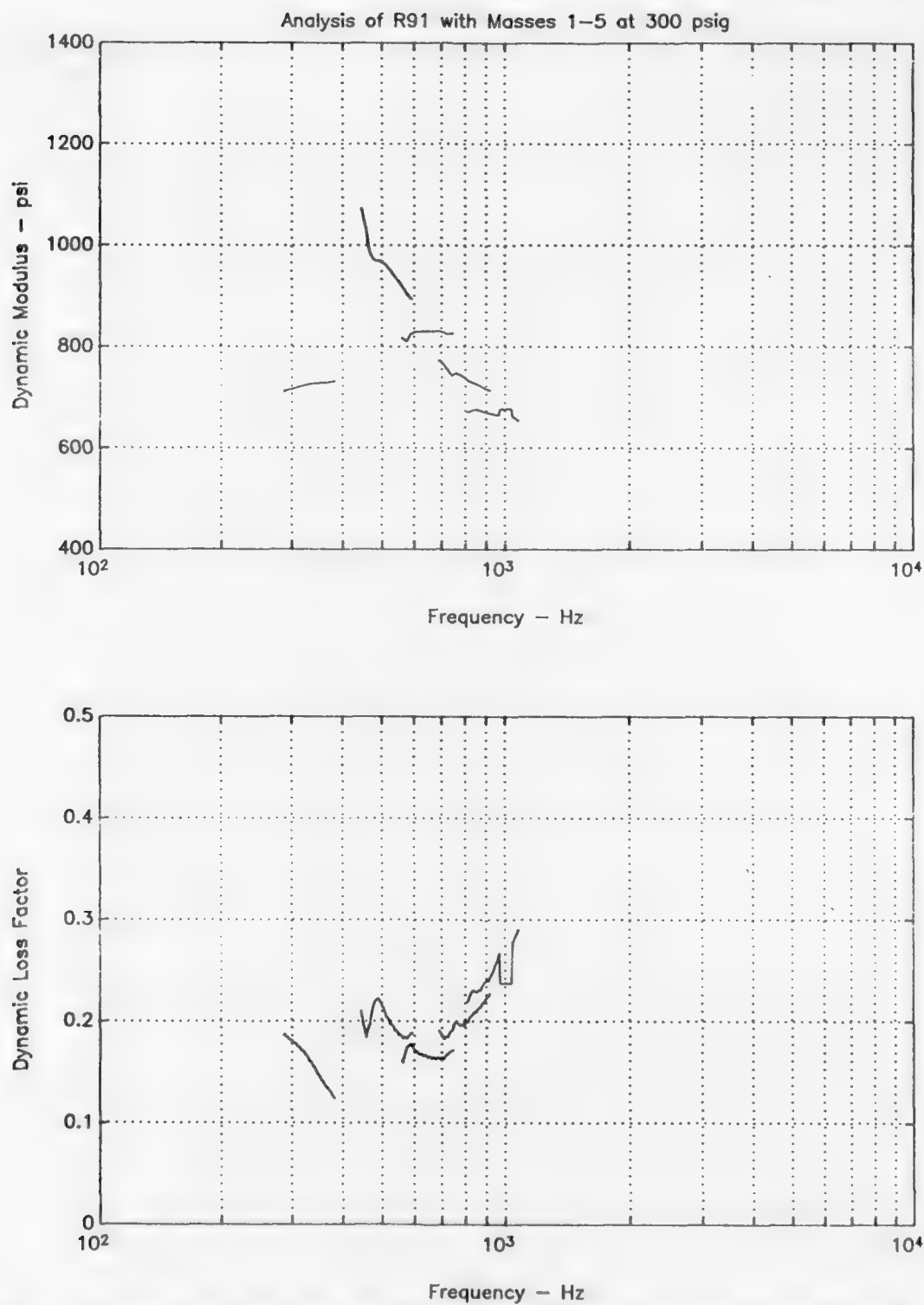

Figure 18.   Dynamic Modulus and Loss Factor for R91 with Masses 1-5 at 300 psig

Figure 19.   Dynamic Modulus and Loss Factor for R91 with Masses 1-5 at 400 psig
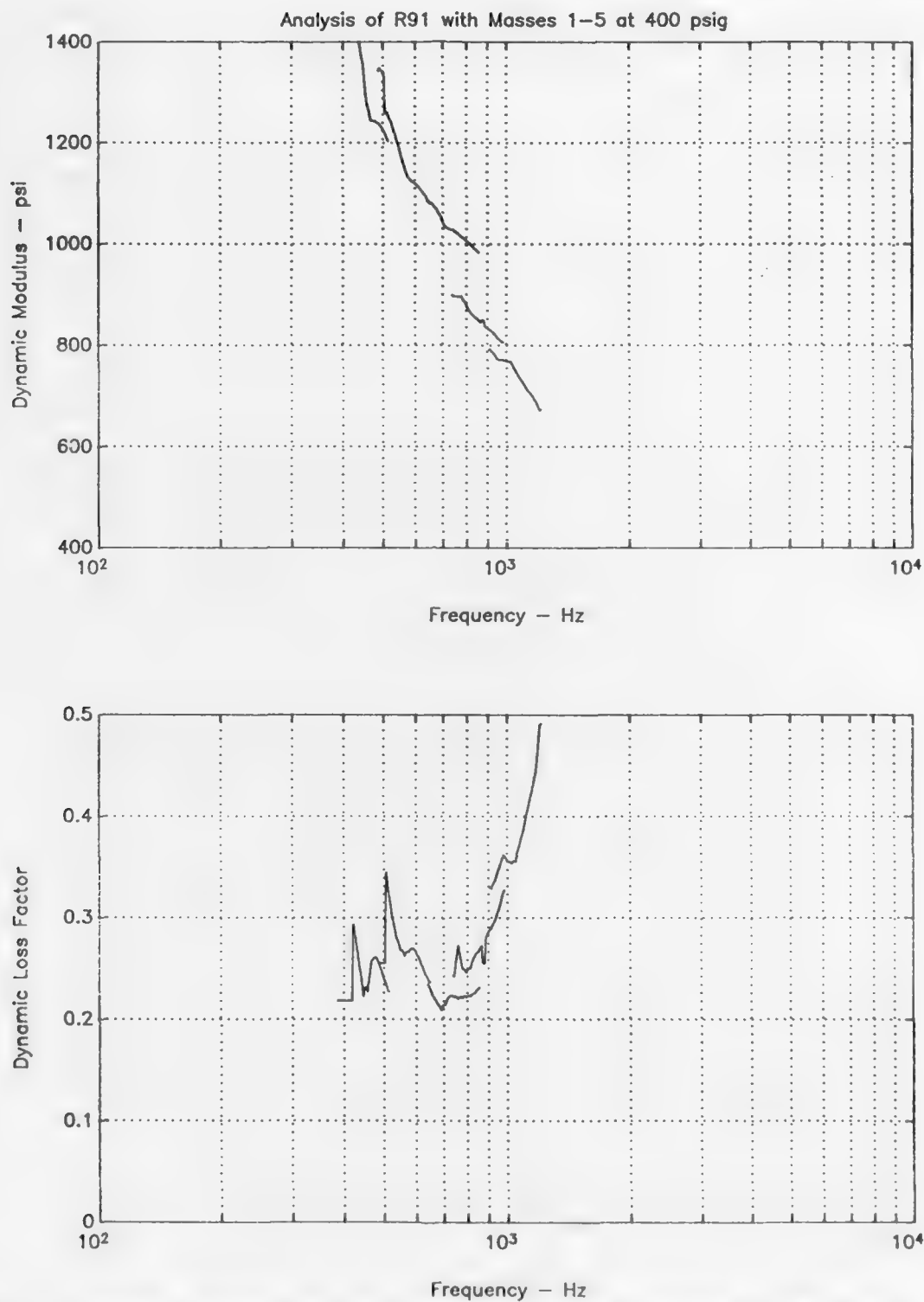
A90 with Mass # 1 from Atm to 400 psig — 22Feb94

Legend
0 — 0 psig
1 — 120 psig
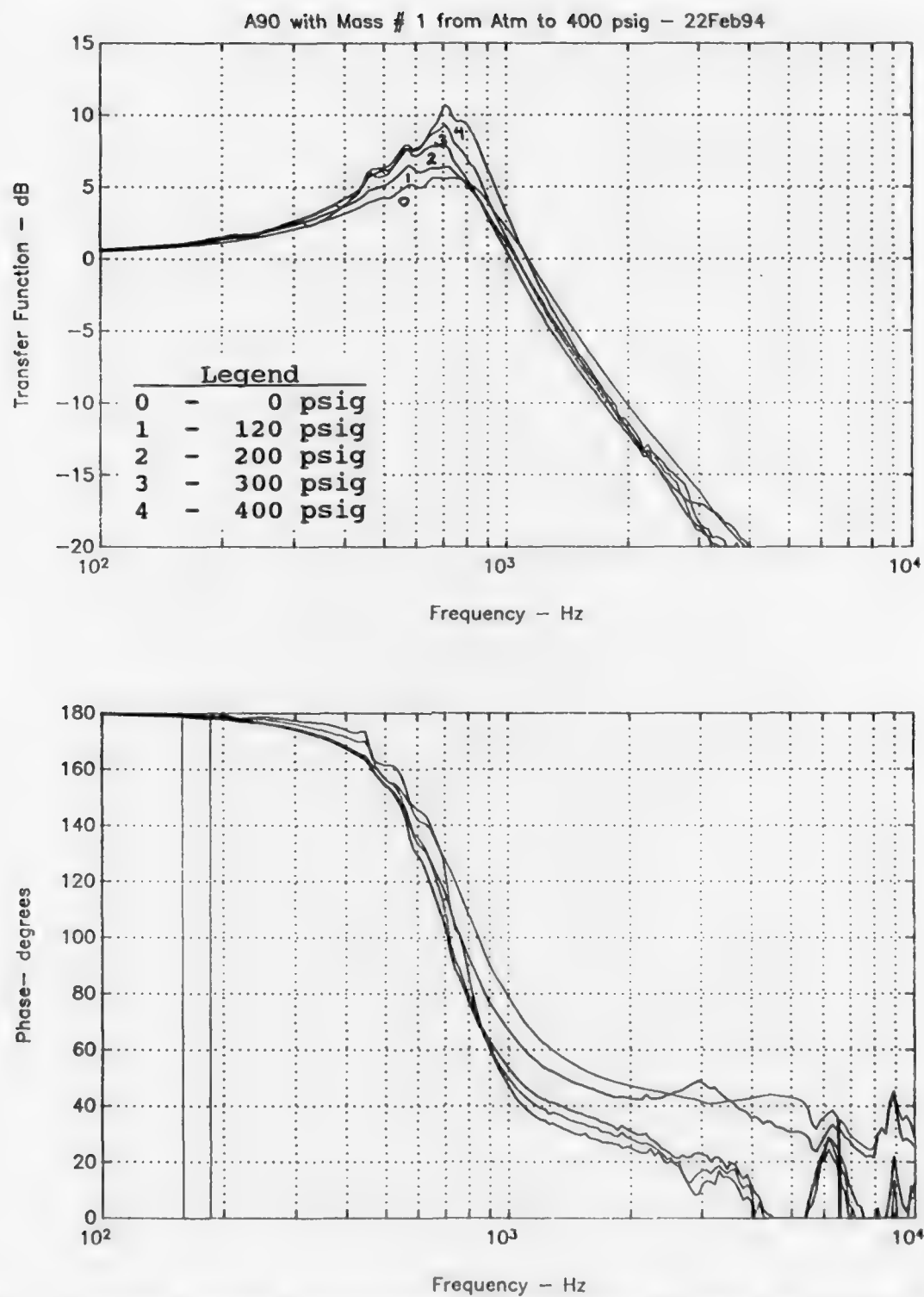2 — 200 psig
3 — 300 psig
4 — 400 psig

Figure 20.   Transfer Function Measurement of A90 with Mass #1 from Atm to 400 psig
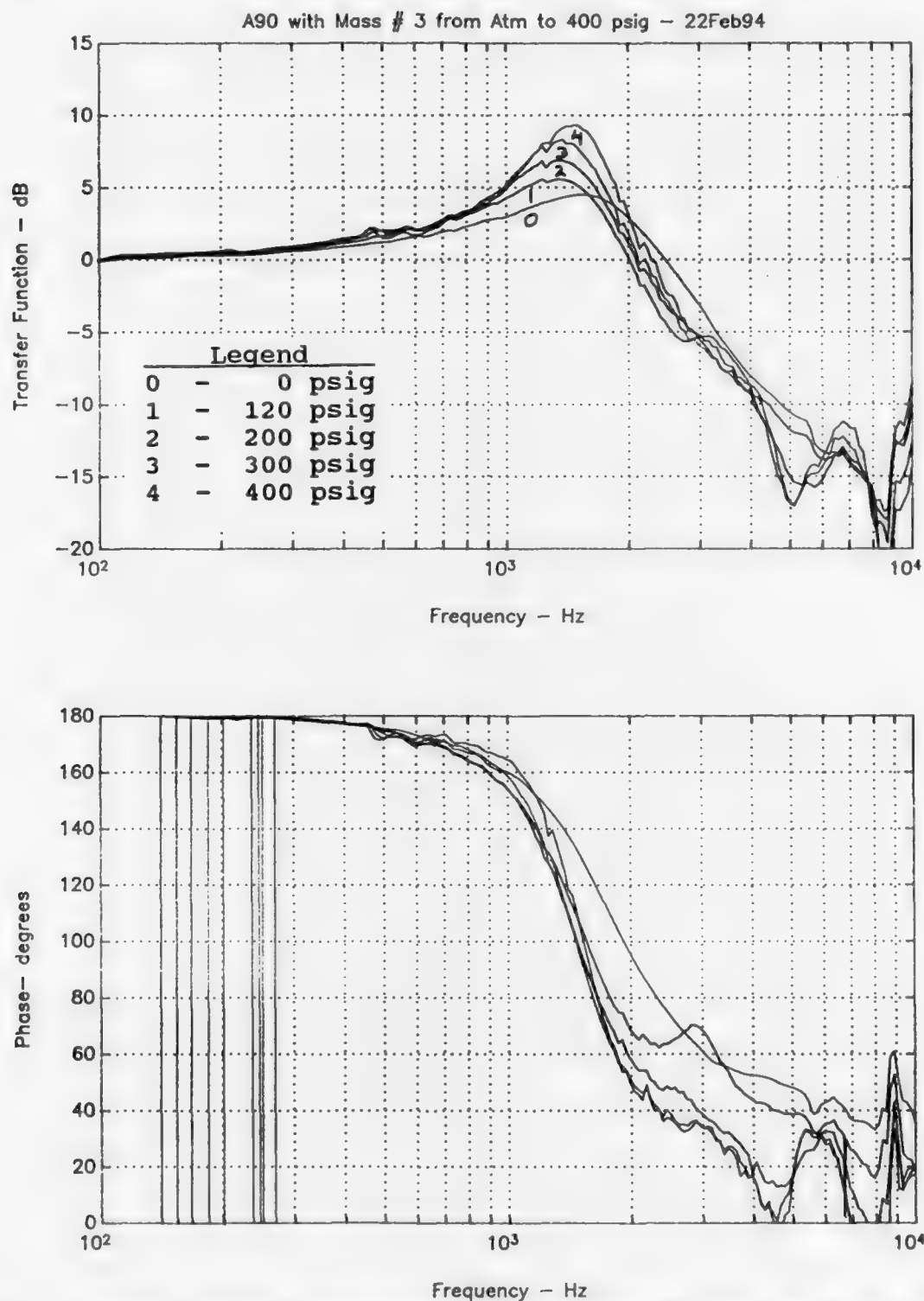
Figure 21.   Transfer Function Measurement of A90 with Mass #3 from Atm to 400 psig
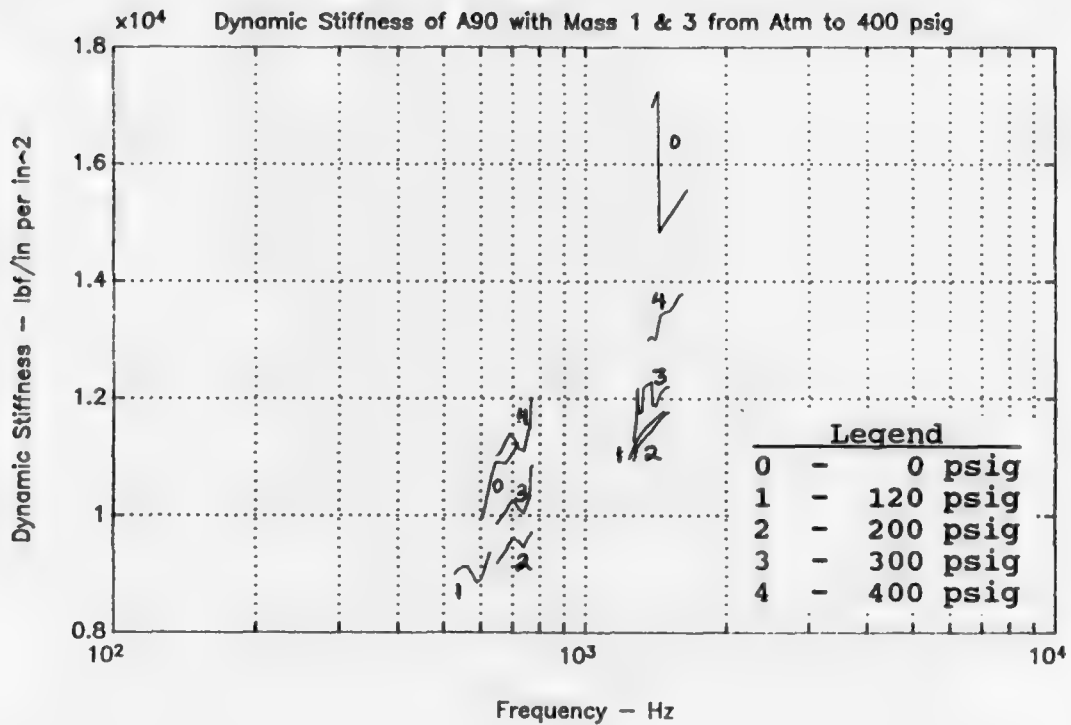
Figure 22.   Dynamic Stiffness of A90 with Masses 1 and 3 from Atm to 400 psig
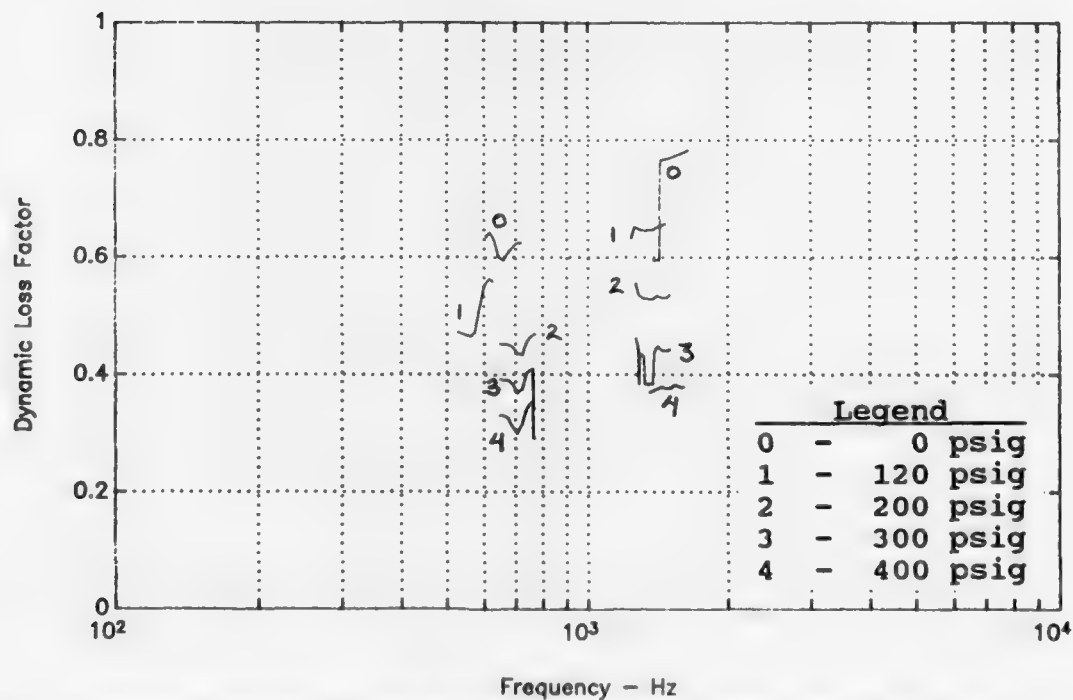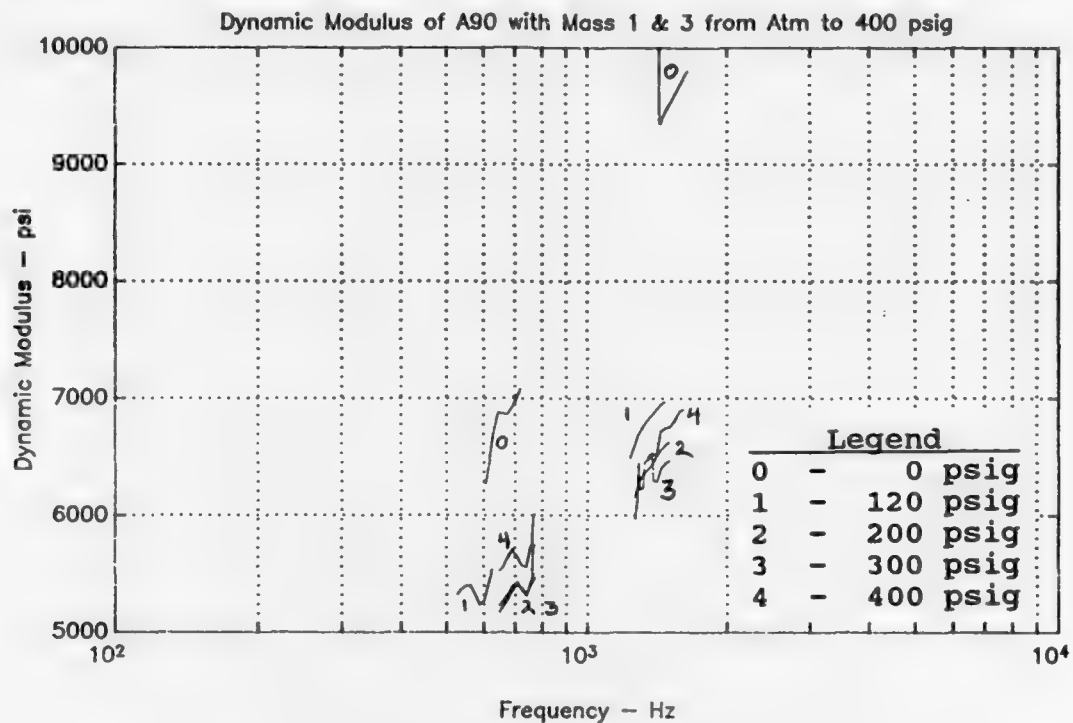
Figure 23.   Dynamic Modulus of A90 with Masses 1 and 3 from Atm to 400 psig

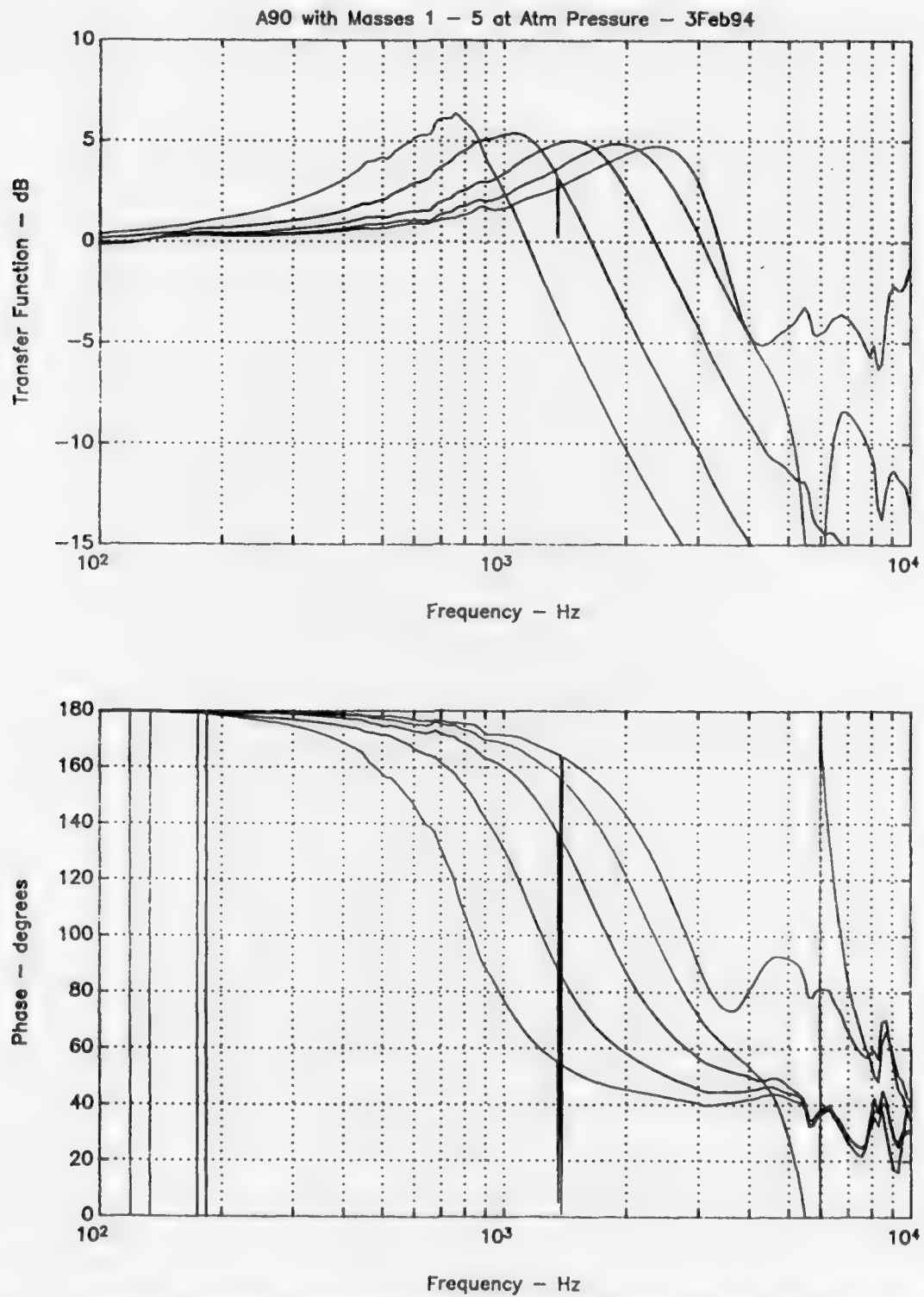A90 with Masses 1 – 5 at Atm Pressure – 3Feb94

Figure 24.   Transfer Function Measurement of A90 with Masses 1-5 at Atm Pressure
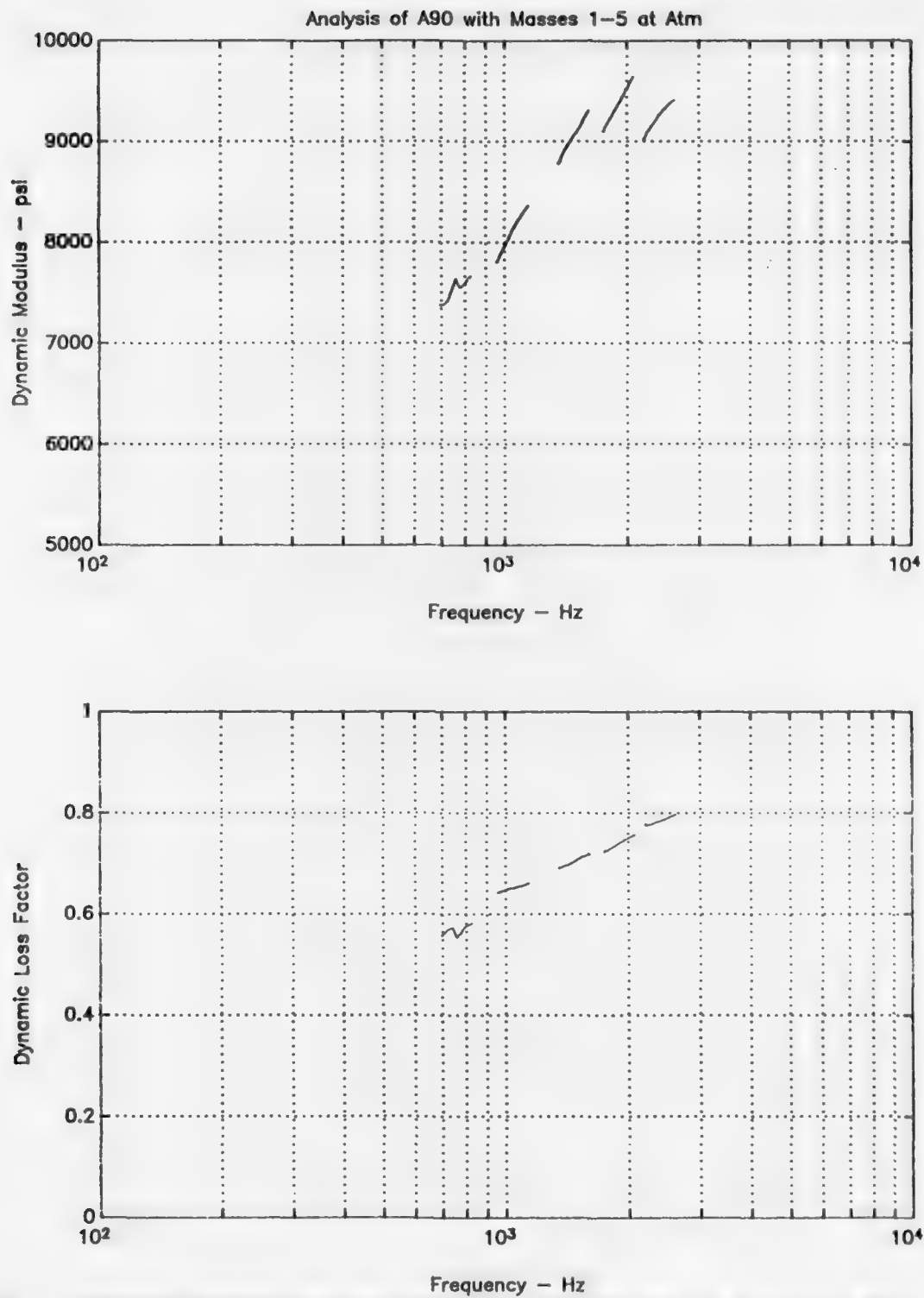
Figure 25.   Dynamic Modulus and Loss Factor for A90 with Masses 1-5 at Atm Pressure

APPENDIX A MATLAB Script Files for Data Analysis

```
%
% This takes the amplitude and phase of the transfer function
% output of the dynamic signal analyzer and computes the complex
% modulus of the data.
%
%
disp(' ')
disp('  DYNAMIC SIGNAL ANALYZER COMPLEX MODULUS ESTIMATE OF DATA')
disp('===========================================================')
disp(' ')
%
freqdata = freqdata';
ampdata = ampdata';
phasedata = phasedata';
%
disp(' Enter a short description of the Test surrounded with single
quotes:');
input('     ');
description = ans;
%
thickness = input('The thickness of the sample: ');
%
density = input('The density of the sample: ');
%
platemass = input('The mass of the top plate: ');
%  add the mass of the fiberglass plate and accelerometer:
fiber = 1.179e-4*(0.13);
accel = 5*(5.71146e-6)/(10.1);
platemass = platemass + fiber + accel;
%
massratio = platemass/(density*thickness);
%
numdata = length(freqdata);
%
%-----------------------------------------------------------------
%   Estimate the real modulus from the resonant peak of data:
%
% AUTOMATIC RESONANT FREQUENCY CALC
[ampmax,index]=max(ampdata);
freqmax=freqdata(index)
ampmax=10^(ampmax/20);
modguess=(platemass*thickness)*(ampmax/(ampmax-1))*(2*pi*freqmax)
^2;
%modguess=(platemass*thickness)*(2*pi*freqmax)^2;
```

44

```
%
modguess=modguess*(1-i*(1/ampmax))
%
%
%--------------------------------------------------------------

%  Assign global variables for use within subroutines:
%
global massratio amp phase;
%
%--------------------------------------------------------------
%  DETERMINE RANGE OF DATA TO CALCULATE MODULUS AND ETA:
%
disp('    Enter 1 to Calculuate Modulus of Data over a Frequency
Range: ');
input('    Enter 2 to Calculuate Modulus of Data Around the
Resonance: ');
m = ans;
%
if m ~= 1,
%
%   LOOP OVER PLUS/MINUS THE RESONANT FREQUENCY:
%
    span = input('The Number of +/- Points around the Resonance: ');
%
    if index <= span,
        ilow = 1;
    else
        ilow = index - span;
    end
%
    if index > numdata-span,
        ihigh = numdata;
    else
        ihigh = index + span;
    end
else
%
%   LOOP FROM USER DEFINED LOW TO HIGH FREQUENCY:
%
  freqlow = input('The Lowest Desired Analysis Frequency: ');
%
  freqhigh = input('The Highest Desired Analysis Frequency: ');
%
    ilow = 0;
    ihigh = 0;
```

```
    for m = 1:numdata
        if freqlow >= freqdata(m),
            ilow = ilow + 1;
        end
        if freqhigh >= freqdata(m),
            ihigh = ihigh + 1;
        end
    end
    span = ihigh - ilow + 1;
end
%
%-------------------------------------------------------------------
% ANALYSIS OF DATA:
%
clear khest modest modulus lossfactor stiffness modfit etafit;
%
% Initilize result vectors below range of analysis with NaN
if ilow > 1,
    for m =  1:ilow-1,
        khest(m) = NaN;
        modest(m) = NaN;
    end
end
%
% Calculate values of "kh" for the range of analysis:
for m = ilow:ihigh,
    omega=2*pi*freqdata(m);
    amp=ampdata(m);
    phase=phasedata(m);
    initial=omega*sqrt(density/modguess)*thickness;
    kh=fzero('xfer',initial);
    if real(kh)<0 | imag(kh)<0,
        freqdata(m)
        disp(' bad root from 1st guess')
        initial=pi/2-eps;
        kh=fzero('xfer',initial);
        if real(kh)<0 | imag(kh)<0,
            disp(' bad root from 2nd guess')
        end
    end
    khest(m) = kh;
    modest(m) = density*(omega*thickness/kh)^2;
end
```

```
%
% Initilize result vectors below range of analysis with NaN
for m =  ihigh+1:numdata,
    khest(m) = NaN;
    modest(m) = NaN;
end
%
% Calculate Modulus and Eta from the estimated values of "kh"
for m = 1:numdata,
    modulus(m)    =  real(modest(m));
    if modulus(m) == NaN,
        lossfactor(m) = NaN;
        stiffness(m) = NaN;
    else
        lossfactor(m) = -imag(modest(m))./modulus(m);
        stiffness(m) = modulus(m)./thickness;
    end
end
%
%*****************************************************************
%
function y=xfer(kh)
%
% This MATLAB function is used with "FZERO" to determine the roots
% of the dynamic equation for a two mass (plate and elastomer
% system used in the Dynamic Signal Analyzer analysis.
%
% The function determines the value of kh in the equation:
%
% 0 = cos(kh) - (mass/rho*h)*(kh)*sin(kh) - (amplitude)e^(i*phase)
%
%---------------------------------------------------------------
%   Function evaluation with sinusoidal representation:
%
%z1=cos(kh);
%z2=(kh)*massratio;
%z3=sin(kh);
%
%---------------------------------------------------------------
%   Function evaluation with exponential representation:
%
z1=(1/2)*(exp(i*kh)+exp(-i*kh));
z2=(kh)*massratio;
z3=(1/(2*i))*(exp(i*kh)-exp(-i*kh));
%
%---------------------------------------------------------------
% Convert the amplitude from "dB space" to real ratio
```

47

```
%    and the phase from degrees to radians and add "pi" to
%    account for the accelerometers being placed 180 degrees
%    out of phase:
%
zamp=10^(-amp/20);
zphase=pi*(phase/180) + pi;
%
z4=zamp*exp(i*zphase);
%
y=z1-z2*z3-z4;
%
```

END

FILMED

DATE: 9- 94

DTIC